

The Gemini NICI Planet-Finding Campaign: The Frequency of Giant Planets Around Debris Disk Stars¹

Zahed Wahhaj², Michael C. Liu³, Eric L. Nielsen³, Beth A. Biller⁴, Thomas L. Hayward⁵,
Laird M. Close⁶, Jared R. Males⁶, Andrew Skemer⁶, Christ Ftaclas³, Mark Chun³,
Niranjan Thatte⁷, Matthias Tecza⁷, Evgenya L. Shkolnik⁸, Marc Kuchner⁹, I. Neill Reid¹⁰,
Elisabete M. de Gouveia Dal Pino¹¹, Silvia H. P. Alencar¹², Jane Gregorio-Hetem¹¹, Alan
Boss¹³, Douglas N. C. Lin¹⁴ Douglas W. Toomey⁷

¹Based on observations obtained at the Gemini Observatory, which is operated by the Association of Universities for Research in Astronomy, Inc., under a cooperative agreement with the NSF on behalf of the Gemini partnership: the National Science Foundation (United States), the Science and Technology Facilities Council (United Kingdom), the National Research Council (Canada), CONICYT (Chile), the Australian Research Council (Australia), Ministério da Ciência e Tecnologia (Brazil) and Ministerio de Ciencia, Tecnología e Innovación Productiva (Argentina).

²European Southern Observatory, Alonso de Cordova 3107, Vitacura, Casilla 19001, Santiago, Chile

³Institute for Astronomy, University of Hawaii, 2680 Woodlawn Drive, Honolulu, HI 96822, USA

⁴Max-Planck-Institut für Astronomie, Knigstuhl 17, D-69117 Heidelberg, Germany

⁵Gemini Observatory, Southern Operations Center, c/o AURA, Casilla 603, La Serena, Chile

⁶Steward Observatory, University of Arizona, 933 North Cherry Avenue, Tucson, AZ 85721, USA

⁷Department of Astronomy, University of Oxford, DWB, Keble Road, Oxford OX1 3RH, U.K.

⁸Lowell Observatory, 1400 West Mars Hill Road, Flagstaff, Arizona, 86001, USA

⁹NASA Goddard Space Flight Center, Exoplanets and Stellar Astrophysics Laboratory, Greenbelt, MD 20771, USA

¹⁰Space Telescope Science Institute, 3700 San Martin Drive, Baltimore, MD 21218, USA

¹¹Universidade de Sao Paulo, IAG/USP, Departamento de Astronomia, Rua do Matao, 1226, 05508-900, Sao Paulo, SP, Brazil

¹²Departamento de Fisica - ICEX - UFMG, Av. Antônio Carlos, 6627, 30270-901, Belo Horizonte, MG, Brazil

¹³Department of Terrestrial Magnetism, Carnegie Institution of Washington, 5241 Broad Branch Road, NW, Washington, DC 20015, USA

¹⁴Department of Astronomy and Astrophysics, University of California, Santa Cruz, CA, USA

¹⁵Mauna Kea Infrared, LLC, 21 Pookela St., Hilo, HI 96720, USA

ABSTRACT

We have completed a high-contrast direct imaging survey for giant planets around 57 debris disk stars as part of the Gemini NICI Planet-Finding Campaign. We achieved median H -band contrasts of 12.4 mag at $0.5''$ and 14.1 mag at $1''$ separation. Follow-up observations of the 66 candidates with projected separation < 500 AU show that all of them are background objects. To establish statistical constraints on the underlying giant planet population based on our imaging data, we have developed a new Bayesian formalism that incorporates (1) non-detections, (2) single-epoch candidates, (3) astrometric and (4) photometric information, and (5) the possibility of multiple planets per star to constrain the planet population. Our formalism allows us to include in our analysis the previously known β Pictoris and the HR 8799 planets. Our results show at 95% confidence that $<13\%$ of debris disk stars have a $\geq 5M_{Jup}$ planet beyond 80 AU, and $<21\%$ of debris disk stars have a $\geq 3M_{Jup}$ planet outside of 40 AU, based on hot-start evolutionary models. We model the population of directly-imaged planets as $d^2N/dMda \propto m^\alpha a^\beta$, where m is planet mass and a is orbital semi-major axis (with a maximum value of a_{max}). We find that $\beta < -0.8$ and/or $\alpha > 1.7$. Likewise, we find that $\beta < -0.8$ and/or $a_{max} < 200$ AU. For the case where the planet frequency rises sharply with mass ($\alpha > 1.7$), this occurs because all the planets detected to date have masses above $5M_{Jup}$, but planets of lower mass could easily have been detected by our search. If we ignore the β Pic and HR 8799 planets (should they belong to a rare and distinct group), we find that $<20\%$ of debris disk stars have a $\geq 3M_{Jup}$ planet beyond 10 AU, and $\beta < -0.8$ and/or $\alpha < -1.5$. Likewise, $\beta < -0.8$ and/or $a_{max} < 125$ AU. Our Bayesian constraints are not strong enough to reveal any dependence of the planet frequency on stellar host mass. Studies of transition disks have suggested that about 20% of stars are undergoing planet formation; our non-detections at large separations show that planets with orbital separation > 40 AU and planet masses $> 3 M_{Jup}$ do not carve the central holes in these disks.

1. INTRODUCTION

Debris disks are second-generation dust disks found mostly around relatively young (0.01–1 Gyr) stars. They are made of collisional debris from planetesimals left over after the primordial dust disks have disappeared (e.g. Zuckerman 2001; Wyatt 2008). Observational studies of debris disks have been a major part of the effort to understand planet formation.

Since the first image of the β Pictoris disk (Smith & Terrile 1984), high-resolution imaging has revealed the morphology of many debris disks. The presence of holes and azimuthal asymmetries in the dust distribution can give clues to the presence of planetary bodies in the disks (e.g. Ozernoy et al. 2000; Wyatt & Dent 2002; Kuchner & Holman 2003). Moreover, the debris disks around younger stars are brighter (e.g. Rieke et al. 2005; Su et al. 2006), a result which provides a constraint on planet formation models. These links to planet formation make debris disks excellent targets for planet searches.

Radial velocity (RV) and transit searches for extrasolar planets have resulted in over 800 discoveries, providing a wealth of information on the frequency of planets with small orbital radii (≤ 5 AU) in old systems (~ 3 Gyr) (e.g. Cumming et al. 2008; Howard et al. 2012). Meanwhile, direct imaging searches have begun to set strong constraints on the population of planets at larger separations, targeting young systems since they have brighter planets. Biller et al. (2007) conducted a study of 54 young nearby stars of spectral types A–M, using the 6.5-m MMT and the 8-m VLT. Selecting somewhat older stars (median age ~ 250 Myr), Lafrenière et al. (2007) obtained adaptive optics (AO) imaging of a sample of 85 nearby stars, using the ALTAIR system on the Gemini North telescope. In a comprehensive statistical analysis of these samples, Nielsen & Close (2010) estimated that 95% of stars have no planets at separations larger than 65 AU, at 95% confidence. Later, Leconte et al. (2010) presented results on a sample of 58 stars, including objects with known disks and known exoplanets, finding that less than 20% of such stars can have $>40 M_{Jup}$ companions between 10 and 50 AU. Janson et al. (2011) have imaged 18 stars of spectral type earlier than A0 and concluded that less than 32% of such systems have planets on wide orbits (however, see discussion in Nielsen et al. 2013). Finally, Vigan et al. (2012) presented a direct-imaging survey which included 42 A and F stars and estimated that 5.9–18% of A and F stars have planets at separations between 5–320 AU (though age estimates for many of their targets were somewhat optimistic; see Nielsen et al. 2013.)

An interesting result of direct imaging searches so far is that many of the systems with exoplanet discoveries also have debris disks, i.e. β Pictoris, HR 8799 and Fomalhaut (Lagrange et al. 2009; Marois et al. 2008; Kalas et al. 2008). Even though the discovery rate for large-separation exoplanets in debris disk systems is low ($<2\%$; this work), the discovery rate in non-debris disk systems is even lower. In addition, Wyatt et al. (2012) find that the RV-discovered systems with only Saturn-mass planets have a higher-than-expected debris disk fraction, 4 out of 6 (67%) compared to 4 of 11 (36%) in the full sample of stars with RV planets (debris disk fraction in RV Jupiter-mass systems is constrained to $<20\%$). The correlation between higher disk fraction and lower-mass planets suggests that the formation mechanism for Saturn-only systems results in large, stable debris disks which can produce dust for a long time, though based on small number statistics.

Since late 2008, the Gemini NICI Planet-Finding Campaign has been conducting a direct-imaging search for exo-planets around a large sample nearby young stars (Liu et al. 2010). In this paper, we present the NICI Campaign results for 57 debris disk stars, the largest and most sensitive direct-imaging search for planets around debris disk systems to date. Companion papers by Biller et al. (2013) and Nielsen et al. (2013) present survey results for the nearby moving group stars and young A & F stars, respectively.

2. OBSERVATIONS

A sample of 57 debris disk stars (Table 1) was observed as part of the NICI Campaign from 2008 to 2012 (see Table 2). The ages, distances and spectral types of the debris disk stars are displayed in Figure 1 and their disk properties are shown in Table 3. A little more than half the stars (29/57) are FGKM stars, while the rest (28/57) are B or A stars. The age estimates for our B and A stars come from a new Bayesian method discussed in Nielsen et al. 2013. The ages for the rest come from the compilations of debris disks in Rieke et al. (2005), Su et al. (2006), Moór et al. (2006) and Rhee et al. (2007). The main methods for estimating the ages can be found in Zuckerman & Song (2004).

The ages of our target stars range from 5 to 1130 Myr with a median of 100 Myr and an RMS of 205 Myr. The distribution is actually bimodal with 25 stars younger than 60 Myr with a median of 12 Myrs and RMS of 12 Myr, and 32 stars older than 60 Myr with a median of 224 Myr and RMS of 220 Myr. The two subsets represent moving group members and older debris disks, and thus our sample is about evenly distributed between the two subsets. The distances to the target stars range from 3.2 to 112 pc. The 15 stars that lie beyond 60 pc are B, A or F stars.

The debris disk stars were observed using our standard Campaign observing modes described in detail in Wahhaj et al. (2013). To summarize, we observed each target in two modes, Angular Spectral Differential Imaging (ASDI) and Angular Differential Imaging (ADI), in order to optimize sensitivity to both methane-bearing and non-methane-bearing companions. In ASDI mode, we imaged simultaneously in the off- (1.578 μm ; CH_4S 4%) and on-methane (1.652 μm ; CH_4L 4%) bands using NICI’s dual near-IR imaging cameras. In ADI mode, we only observed in the H -band using one camera. The ASDI mode is more sensitive to companions at separations less than $\sim 1.5''$, while the ADI mode is more sensitive at larger separations. In both observing modes, the primary star was placed behind a partially transmissive focal plane mask with a half-power radius of 0.32'' and a full extent of 0.55''.

When using the ADI technique, the telescope rotator is turned off, and the sky rotates with respect to the instrument detectors. This is done so that the instrument and the telescope optics stay aligned with each other and fixed with respect to the detector. Their respective speckle patterns, caused by imperfections in the optics, are thus decoupled from any astronomical objects. When reducing images, a reference PSF made by stacking the speckle-aligned images was subtracted from the individual images, so that some fraction of the speckle pattern was removed. At large separations from the target star ($\gtrsim 1.5''$), our sensitivity is limited by throughput not by residual speckle structure. Thus in the ADI mode, all the light is sent to one camera in order to achieve maximum sensitivity. We usually obtained 20 1-minute images using the standard *H*-band filter, which is about four times wider than the 4% methane filters.

To search for close-in planets, we combined NICI’s angular and spectral difference imaging modes into a single unified sequence that we call “ASDI”. In this observing mode, a 50-50 beam splitter in NICI divides the incoming light between the off- and on-methane filters which pass the light into the two imaging cameras, henceforth designated the “blue” and “red” channels respectively. The two cameras are read out simultaneously for each exposure and thus the corresponding images have nearly identical speckle patterns, which can be subtracted from each other, prior to ADI processing. In the ASDI mode, we typically obtain 45 1-minute frames.

3. DATA REDUCTION

The Campaign data reduction procedures are described in detail in Wahhaj et al. (2013). Briefly, in our standard ASDI reduction, we reduce the images in five steps: (1) do basic reduction of flatfield, distortion and image orientation corrections; (2) determine the centroid of the primary star and apply image filters (e.g. smoothing); (3) subtract the red channel from the blue channel (SDI); (4) subtract the median of the entire stack of images from the individual difference images (ADI); and (5) de-rotate each individual image to a common sky orientation and then stack the images. The ADI reduction is the same as the ASDI reduction, except that since we are only dealing with the blue channel images, we do not perform the SDI reduction in step 3.

Flatfield images have been obtained during most NICI Campaign observing runs, and thus most datasets have corresponding flatfields obtained within a few days of their observing date. The images are divided by the flatfield, which we estimate to have an uncertainty of 0.1%. This was estimated from the fractional difference between separate flatfields made from two halves of a sequence of flatfield images.

In NICI Campaign datasets, the primary star is usually unsaturated as it is imaged through a focal plane mask which is highly attenuating ($\Delta CH_4(4\%)S = 6.39 \pm 0.03$ mag, $\Delta CH_4(4\%)L = 6.20 \pm 0.05$ mag, $\Delta H = 5.94 \pm 0.05$ mag; Wahhaj et al. 2011). Thus the locations of the primary star in these images are accurately determined and used later for image registration. The centroiding accuracy for unsaturated peaks or peaks in the non-linear regime is 0.2 mas (Wahhaj et al. 2013) or 1% of a NICI pixel. In ASDI datasets for bright stars ($H < 3.5$ mag) and in most ADI datasets, the primary is saturated. In these images, the peak of the primary is still discernible as a negative image. The pixel with the smallest value in the negative image is taken to be the centroid. We have estimated that the centroiding accuracy of the saturated images is 9 mas by comparing the estimated centroids in these images to those of the unsaturated short-exposure images obtained right before and after the long exposures.

4. RESULTS

4.1. Contrast Curves

For each of the reduced data sets, the companion detection sensitivities are presented as 95% completeness contrast curves in delta magnitudes as a function of separation from the primary star. Wahhaj et al. (2013) describe how the 95% completeness limits are defined and measured: 95% of all objects in the field brighter than the indicated contrast level should be detected by our observations. We have previously shown that the 95% contrast curve in most cases agree well (at the ~ 10 – 30% level) with the nominal 5σ contrast curves which are usually presented in direct imaging analyses. We use the 95% curves in this paper, because they are statistically more meaningful and also more reliable.

These completeness curves are calculated by using the unsaturated images of the primary, seen through the coronagraphic mask, as simulated companions. The simulated companions are embedded into the raw images and recovered in the final reduced images using fixed (automatic) detection criteria, as described in Wahhaj et al. (2013.) The companions are inserted into the images with separations such that they do not interfere with each other during ADI processing. For this paper, we will use the term *contrast curve* to mean *95% completeness contrast curve*.

In a few data sets, a bright stellar companion reduced the contrast achieved in some portion of the field. For simplicity, we consider these low contrast regions (worse than the median contrast in an annuli by ≥ 1 mag) as regions without data. For each angular separation we also report the coverage fraction, or the annular fraction with data (Table 4).

Because the primary was not usually placed in the center of the detector, the coverage fraction also falls off gradually at separations $\geq 7''$.

The median contrasts achieved for the debris disk sample at 0.5, 1.0, 2.0, 4.0'' were 12.4, 14.1, 15.5 and 16.2 mag with standard deviations of 0.5, 0.82, 0.87 and 1.3 mag, respectively, across all contrast curves. For separations less than 1.5'', the contrast curves from the ASDI reduction are usually more sensitive than those from the ADI reduction. For larger separations, the ADI contrast curves are more sensitive. If the images are saturated for one reduction, we report the contrast curve from the other reduction(s) for the relevant separations. When estimating sensitivities to planets, we use all available contrast curves independently, as described in § 4.6. We report our final contrasts in Table 4 and Figure 2. The companion mass limits corresponding to these contrasts are presented in Table 5, along with the mass limits at the debris disk edges. The brightness to mass conversions are obtained using the hot-start models in Baraffe et al. (2003a).

4.2. Follow-up of Candidate Companions

Many candidate companions were detected in our observations. The targets with candidates were observed again several months to years later to check if the candidates were comoving with the primary or were fixed in the sky as expected for background objects. Usually, a second-epoch observation was obtained only when the expected relative motion between the science target and any background star was more than about 3 NICI PSF widths (150 mas). The primary's motion was calculated from its proper motion and parallax, usually from the revised Hipparcos Catalog (van Leeuwen 2007). Multiple epochs of follow-up observations were obtained when the astrometric uncertainties were too high to determine if candidates were background from the second epoch data. The uncertainties in the separation and PA for each epoch are estimated to be 0.009'' and 0.2° respectively when the primary is unsaturated, and 0.018'' and 0.5° when the primary is saturated (Wahhaj et al. 2013).

We detected a total of 78 planet candidates around 23 stars. Follow-up observations of 19 targets with 66 of the most promising candidates (projected separation < 500 AU) show that all of them are background objects. The astrometry and photometry for these objects are presented in Table 6 and 7. Figures 3–6 show the motion of all the candidates with respect to the primary. The candidates with large projected separation (> 500 AU) were treated as lower priority follow-up targets and thus second-epoch observation of some of these have not been obtained. The astrometry for the 12 candidates around 4 stars which were not followed up are presented in Table 8, along with their projected physical separations in AU. We discuss how our statistical formalism correctly treats these single-epoch detections

in §4.8.

4.3. Contrast limit at the location of Fomalhaut b

Kalas et al. (2008) presented the detection of a planet at 0.6 and 0.8 μm around Fomalhaut using the Hubble Space Telescope (see also Currie et al. 2012; Galicher et al. 2013). The planet was detected at a separation of 12.61'' and a PA of 316.86° in 2004 and a separation of 12.72'' and 317.49° in 2006. The planet was not detected in their H -band or CH_4S -band images obtained in 2005 with 3σ detection limits of $H=22.9$ mag and $CH_4S=20.6$ mag. In this section, we present the detection limits achieved at the location of the planet in a NICI observation obtained on UT 2008 November 17.

In the 2008 NICI observations of Fomalhaut, we placed Fomalhaut in one corner of the NICI detector (only 3.4'' from either edge), so that the location of the planet would lie near the center of the 18.43'' wide detector. We imaged Fomalhaut through the 0.9'' coronagraphic mask in the CH_4L 4% filter with the blue camera only. We obtained 79 images, each with 66.9 seconds of exposure (1.47 hours total). We also obtained an unsaturated short exposure image with an exposure time of 0.38 seconds ($\times 10$ coadds) in the CH_4S 1% filter. The long exposure images are saturated out to a separation of $\sim 1.2''$. The total rotation obtained in the ADI data set was 6.33°, from which we estimate that the planet would move through ~ 25 NICI PSF FWHMs relative to the detector. Thus, we expect almost no self-subtraction of the planet during the ADI image processing. Moreover, the planet would only change position by 0.33 PSF cores between adjacent exposures, and thus smearing during an individual exposure on the detector was also negligible. The airmasses for the observation ranged from 1.04 to 1.33.

The location of the primary was measured from the saturated images, where the peak of the star can be recognized as a negative image as described in Wahhaj et al. (2013). The precision of these measurements has been estimated to be ~ 9 mas. The images were reduced using the standard ADI Campaign pipeline (Wahhaj et al. 2013). No sources were detected in the reduced image near the locations of the Kalas et al. (2008) detections or anywhere else in the image.

To determine the contrast limit near the location of the Kalas et al. (2008) planet, we needed to measure the opacity of the 0.9'' focal plane mask in the CH_4S 1% filter. This was done by scanning a calibration light source internal to the AO system across the mask and measuring the change in its relative brightness. As a result, the opacity at the center of the mask was measured to be 6.2 ± 0.1 mag.

To estimate the contrast at the location of the planet, we simulated planets by scaling the star spot in the short exposure image to different contrasts relative to the primary and inserted them into the raw images. The simulated planets were inserted at 25 locations in a sector of the image, of radial extent $2''$ and total PA extent 10° ($\sim 2.2''$ arc length). The sector was centered near the location of the planet at a separation of $12.65''$ and a PA of 317° . We determine the contrast at which all 25 planets are recovered according to the procedure described in Wahhaj et al. (2013). This procedure was repeated four times, changing the center of the insertion region by $0.1''$ each time in the positive and negative separation and PA directions. In this way, we determine the contrast at which $>99\%$ (100 out of 100) planets are recovered near the location of Fomalhaut b. This contrast is 20.2 mag (ΔCH_4S 1%). In Figure 8, we show the location of Kalas et al. (2008) detections and the simulated planets at the contrast limit of the reduced image.

The Strehl ratio of the NICI images were degraded with increasing angular separation from the primary due to anisoplanatism, but we do not have an independent estimate of the degradation for NICI observations. In the absence of anisoplanatism data for Gemini-South, we simply follow Lafrenière et al. (2007) and assume that the reduction in Strehl for the ALTAIR AO system is $e^{-(\text{separation}/12.5)^2}$, with the separation in arcseconds, or 1.1 mag at the location of the planet. We apply this correction to the contrast curves and assume an uncertainty of 0.3 mag. For Fomalhaut, $V = 1.16$ (SIMBAD) and $V - H = 0.28$ (A4V star Kenyon & Hartmann 1995). Assuming $H - CH_4S = 0$, we get $CH_4S = 0.88$ mag for the primary star. Adding the contrast limit and Fomalhaut’s brightness, we estimate with 99% confidence that there are no planets at the location of Fomalhaut b with $CH_4S < 20.0 \pm 0.3$ mag. We do not improve much on the $CH_4S > 20.6$ contrast limit presented in Kalas et al. (2008), although we note that the contrast quoted therein was a nominal 3σ limit, obtained without testing with simulated planets. In Figure 8, we plot the nominal 5σ contrast curve for our 2008 Fomalhaut dataset scaled to match the contrast measurement at the location of the planet. Inside of $1.8''$ separation, we plot the contrast curve from a UT 2011 October 12 ASDI data set.

Using the Baraffe et al. (2003b) models, Fomalhaut’s Hipparcos parallax of 129.81 mas and assuming an age of 450 ± 40 Myr for Fomalhaut (Mamajek 2012), we estimate an upper limit of $12\text{--}13M_{Jup}$ for the mass of the planet from our CH_4S non-detection. This is well above the dynamical mass estimate of $< 3M_{Jup}$ presented in the 2008 discovery paper, and the upper limit of $< 2M_{Jup}$ from the $4.5 \mu\text{m}$ and J -band non-detections (Janson et al. 2012; Currie et al. 2012). Thus, it is not surprising that we do not detect the planet.

4.4. Especially Low Mass-limits Achieved within 15 AU

Especially high-sensitivities to planets within 15 AU projected separation were achieved for GJ 803 ($4M_{Jup}$ at 5 AU; $2.5 M_{Jup}$ at 10 AU), and β Pic ($6.5 M_{Jup}$ at 10 AU; β Pic b was detected interior to this separation). High sensitivities were also achieved for TWA 7 ($4 M_{Jup}$ at 14 AU), HIP 25486 ($5 M_{Jup}$ at 13 AU), HD 17255A ($6 M_{Jup}$ at 15 AU), Fomalhaut ($10 M_{Jup}$ at 15 AU) and ϵ Eridani ($11 M_{Jup}$ at 10 AU). Although these are higher sensitivities than achieved in previous surveys, we are not yet sensitive to true Jupiter-analogs. However, such sensitivities have already been obtained in the one special case of AP Col, a very nearby (8.4 pc) young (12–50 Myr) M-dwarf. (Quanz et al. 2012).

4.5. Bayesian Inference on Planet Populations

In this section, we constrain the population of extrasolar planets around nearby debris disk stars using Bayesian statistics. Bayes’ equation tells us that

$$P(model | data, I) = P(data | model, I) \frac{P(model | I)}{P(data | I)}, \quad (1)$$

where $P(data | model, I)$ is the probability of the *data* given the *model* and *I* is any relevant prior information we have about our targets and our observations. The *model* is our hypothesis about the planet population expressed in terms of some interesting parameters, such as the average number of planets around AFGKM type stars. The *data* are relevant information from the observations which most strongly constraint the interesting parameters.

In our case, there are two interesting model parameters to constrain using our observations: (1) the frequency of planets (average number of planets around a sample star) and (2) the fraction of stars with at least one planet. For both parameters, we are considering stars with detected debris disks and planets in a certain mass and semi-major axis (SMA) range, as these are the fundamental constraints from our dataset.

4.5.1. The Frequency of Giant Planets

We model the probability distribution of the number of planets in a single system as a Poisson distribution:

$$P(n | F) = \frac{1}{n!} F^n e^{-F}, \quad (2)$$

where n is the number of planets in the system and F is the expectation value of the distribution i.e., the frequency of planets which is one of the model parameters of interest.

For the j th star in our sample of N stars, we use f_j to denote the fraction of planets that are detectable in a certain mass and SMA range, given that such planets are distributed according to some population model. These f_j are calculated using the contrast limits for the j th star and Monte Carlo simulations as in Nielsen & Close (2010). Thus nf_j is the expectation value of the number of planets detected for a system with n planets. Let n_j be the number of planets actually detected for that star. Then the likelihood for n_j detections given that nf_j is the expected value is given by another Poisson distribution:

$$P(n_j | nf_j) = \frac{1}{n_j!} (nf_j)^{n_j} e^{-nf_j}. \quad (3)$$

We would like to determine the model parameters, F and n . The contrast curve for the j th star and the data are $\{c_j\}$ and $\{n_j\}$, respectively. However the contrast curves are only relevant to calculating the f_j 's and thus $P(n_j | n, c_j)$ is the same as $P(n_j | nf_j)$, the probability of n_j detections given that n planets exist and a fraction f_j of a model population are above the contrast limits.

Thus, using Bayes's equation we get

$$P(F, n | \{n_j\}, \{c_j\}, I) = \prod_{j=1}^N P(n_j | nf_j) P(n | F). \quad (4)$$

This expression is exact under certain assumptions: (1) the observation result from one star does not affect the information we have another star and (2) the priors $P(n_j, f_j | I)$, $P(n_j | f_j, I)$, $P(f_j | I)$, $P(f_j | F, n, I)$ are flat (=1) because we have no information about them. The Appendix provides a complete derivation of Eq. 4.

We obtain the probability distribution for the frequency of planets, F , by summing over the parameter, n .

$$P(F | \{n_j\}, \{c_j\}, I) = \prod_{j=1}^N \left(\sum_n P(n_j | nf_j) P(n | F) \right). \quad (5)$$

We could sum n from zero to infinity to be exact. However, the calculations will be sufficiently precise when the upper bound is large compared to the maximum number of actual detections in a single system. So, we sum n from zero to 20.

For any star with multiple planets, we have to use the above general expression. However for our stars, $n_j = 0$ because we did not detect any planets, except in the case of β Pic b where we count the known planet (astrometry and photometry taken from Bonnefoy et

al. 2013). When we have zero detections ($n_j = 0$), the general expression given by Eq. 4 simplifies to

$$P(F, n \mid n_j = 0, f_j, I) = \sum_n \frac{1}{n!} F^n e^{-(F+nf_j)}. \quad (6)$$

4.5.2. The Fraction of Stars with Planets

Another number of interest is the fraction of stars with planets, which can be derived from F , if we assume a Poisson distribution for the multiplicity of planets as in Eq. 2. The fraction of stars with planets, $F_{sp} = 1 - F_{s0}$, where F_{s0} is the number of stars with zero planets. But $F_{s0} = P(F \mid n = 0) = e^{-F} \Rightarrow F_{sp} = 1 - e^{-F}$. Thus, we can easily derive $P(F_{sp} \mid data, I)$ from $P(F \mid data, I)$, or the probability distribution for the number of stars with planets from that of the frequency of planets, F . In previous work, the fraction of stars with planets has been equated to F (Lafrenière et al. 2007; Vigan et al. 2012) (See Appendix for further discussion of previous work). However, this is only true in the special case that all stars have at most one planet or when $F \ll 1$ (substituting in $F_{sp} = 1 - e^{-F}$).

We will later employ a simpler statistical formulation in which we constrain only the average number of planets per star for the given sample. However, such an approach would not distinguish between different multiplicities of systems, and we would not be able to estimate the fraction of stars with zero planets. In other words, this approach provides weaker constraints on the model population as we are throwing away multiplicity information. The simple formulation would be

$$P(F \mid data) = P(n_d \mid n_m) = \frac{1}{n_d!} e^{-n_m} n_m^{n_d}, \quad (7)$$

where $n_m = \sum_{j=1}^N F f_j = F \sum_{j=1}^N f_j$ is the total number of planet detections predicted by the model. In other words, the number of detections predicted by the model is the detection probability given that exactly one planet exists, times the average planet multiplicity, summed over all stars. Also, n_d is the total number of planets detected in the sample.

This is in fact the likelihood used in Nielsen et al. (2008) and Nielsen & Close (2010) for the case of zero planet detections. We show in § 4.7 that if the distribution of planet multiplicities is in fact Poissonian, then this likelihood can be used to obtain the correct result even if there are actual planet detections in a survey.

4.6. Monte Carlo Simulations to Calculate Detection Probabilities

In this section, we calculate the f_j values (the planet detection probabilities given exactly one planet exists around each star) in our Bayesian formulation employing a Monte-Carlo technique (see Nielsen et al. 2008). For each star j , f_j is the probability of detecting a planet within some chosen mass and SMA range, $m = [m_0, m_1]$ and $a = [a_0, a_1]$, given that exactly one planet exists in that range and that no planets exist at larger a . For each star, we simulate 10^4 planets with a distribution given by

$$\frac{d^2N}{dMda} = n_{11}m^\alpha a^\beta.$$

The 10^4 planets are only assigned masses between 0.5 and 13 M_{Jup} and SMA between 0.5 and 1000 AU. Initially, we set $\alpha = -1.31$ and $\beta = -0.61$, using the estimates from RV surveys (Cumming et al. 2008).

The quantity n_{11} is the number of planets per star per unit mass range and SMA range. From the RV results, we calculate n_{11} to be 0.044. Thus once we have constraints on α and β , we will have estimates for the number of planets in any m and a range, and also be able to compare our results with those from the RV surveys. If they are not consistent we can hypothesize that the planet formation behavior changes beyond some physical regime (e.g. for large SMA). We note here that the f_j computations do not depend on n_{11} .

Next, we transform the m and a values of the simulated planets to ΔH and ρ , the flux ratios and their angular separations relative to their primary stars, respectively. The calculation from a to ρ is performed using the distance to the primary and samplings from prior distributions in orbital parameters and random viewing angles as described in Nielsen et al. (2008). The calculation from m to ΔH is performed using Baraffe et al. (2003a) models also as described in Nielsen et al. (2008). The models use a “hot-start” initial condition for the evolution of planet fluxes with age. In Figure 10, we show the mass sensitivity limits achieved at 0.5'' and 3'' using the Baraffe et al. (2003a) models. It is evident that the contrast achieved at the two separations probe significantly different planet masses. Nielsen & Close (2010) have shown the consequences of using the core-accretion models of Fortney et al. (2008). These “cold start” models predict much lower near-infrared fluxes for planets at ages below 100 Myrs, but agree with the “hot start” models at older ages. However, given the discoveries of the planet around β Pictoris and the four planets around HR 8799, it is evident that at least some planets have luminosities comparable to those produced by “hot start” models (Fabrycky & Murray-Clay 2010).

Now we calculate what fraction of the planets have ΔH and ρ above the NICI imaging contrast limits. For the j th star, this fraction is our desired f_j value. In Figure 9, we

illustrate the computation of f_j , the detection probability of a planet given that only one planet exists for the case of 49 Cet. The detection probabilities for our survey stars ranged from 1% to 30%.

4.7. Limits on the Average Number of Planets around Debris Disk Stars

When we have actual detections, the number of detections in each $\{\Delta H(\rho), \rho\}$ bin should be compared to the number of planets predicted by our number distribution model in those bins. Otherwise our model parameters, α , β , etc. will not be optimally constrained as we will be ignoring information about the brightness and separation of the detected planets. In the case of zero detected planets, however, the likelihood expression for the model parameters is exactly the same, whether we count the predicted detections in each bin separately or count the detections in all the bins together.

For our survey we only have one detection, the known planet around β Pictoris. Thus, we start with the simplest statistical formulation for the average planet multiplicity, F . As we discussed earlier, in this Poissonian formulation we only compare the total number of planet detections expected to the total number actually detected. Then from F , we can calculate F_{sp} the fraction of stars with planets, as described in §4.5.2.

We compute the probability distributions for F and F_{sp} in the two ways, one using the full likelihood and the other using the simple likelihood. For both methods, we have set $\alpha = -1.31$ and $\beta = -0.61$ based on Cumming et al. (2008). First, we consider the entire planet mass and SMA range from 0.5 to $13M_{Jup}$ and 0.5 to 1000 AU, respectively. From Figure 11, we can see that the 2σ upper limit on the average number of planets around our debris disk sample is 0.42, for the chosen range of mass and SMA. Assuming a Poisson multiplicity distribution, the upper limit on F_{sp} is then 35%. The lower limit of 2% is entirely due to the β Pictoris planet detection.

As a check on the validity of both methods, Figure 11 also compares the results obtained from the simple likelihood to the full likelihood derived in §4.5.1. Interestingly, the results from the two likelihoods are quite similar. Although the simple likelihood cannot constrain the multiplicity distribution, if we assume a Poisson distribution, we obtain a good result. Of course, if the real planet multiplicity distribution is not Poissonian, the simpler likelihood will incorrectly yield better constraints than the full likelihood.

As another check, we conducted a simulation with the number of planets and detections around each star following a Poisson distribution. To make matters simple, brightnesses and separations were not simulated, just the number of planets were. Thus, to each star in our

survey, we assigned a number of planets drawn from a Poisson distribution with mean of 3. The number of detections for the star is then just f_j times the number of planets around the star. Figure 12 shows that the results from the two likelihoods are quite similar. Again, although the simple likelihood cannot constrain the multiplicity distribution, if we assume a Poisson distribution, we obtain a good result.

Figure 13 shows the same upper limits computed as a function of planet mass and orbital semi-major axis. In this case, we ignored the power-law model for the distribution of the planets and simply computed the upper limit to the average number of planets in a given $\{m, a\}$ bin. Of course, the likelihood for F in a particular bin cannot be calculated ignoring the average multiplicity outside that bin, unless we stipulate that there are no planets outside. Since we are interested in the absolute upper limit to the number of planets in a bin, we do make that stipulation.

Based on Figure 13, at the 95% confidence level we state that <10% of debris disk stars have a $\geq 5M_{Jup}$ planet at 60 AU, and <30% of debris disk stars have a $\geq 3.5M_{Jup}$ planet at 20 AU. Also, the average number of planets with masses above $3.5M_{Jup}$ at 10 AU is less than 1, and at 25 AU it is less than 0.25. In all cases, only smaller fractions are permitted at larger semi-major axes (up to 500 AU).

4.8. Limits on the Mass and Semi-Major Axis Distribution of Planets

We now consider how our observations constrain α , β and the average planet-multiplicity, if we ignore the constraints from the RV studies both for these parameters and the average planet-multiplicity. Moreover, we add an additional parameter, the SMA cutoff, a_{max} , beyond which no planets are allowed.

The joint probability distribution for the four model parameters is given by

$$P(\alpha, \beta, a_{max}, F|data) = P(data|\alpha, \beta, a_{max}, F) * P(\alpha, \beta, a_{max}, F)/P(data)$$

and again the ratio of priors, the last factor in above expression, is set to unity. The data are as usual the contrast curves and the detections. In calculating the likelihood, $P(\alpha, \beta, a_{max}, F|data)$, the actual and model-predicted detections in each ΔH and ρ bin are compared separately. This requires that for each combination of $\alpha, \beta, a_{max}, F$, we calculate the f_j for each ΔH and ρ bin separately.

Here, single-epoch detections which could neither be confirmed nor rejected as planets are also taken into account. For example, suppose for a certain star, a $\{\Delta H, \rho\}$ bin has n_c candidate companions (from single-epoch detections) and n_d confirmed planet detections.

Suppose also that the planet population model predicts n_m planets in that bin. Then the probability of the available information being true given the model is $\sum_{n_p=n_d}^{n_d+n_c} P(n_p|n_m)$, where P is the Poisson distribution. In other words, we sum the probabilities for the range of possible planets in that bin.

To illustrate the value of including single epoch detections, we consider an observation that tells us that a range of planets are possible for a certain star. This observation therefore contributes equal probabilities to all models which predict planets within that range. Thus, the observation is a poor discriminant for those models. The probability contribution from each star is calculated separately and then multiplied (see Equation 5). Thus, when a star with many candidate planets is added to a survey, it does not weaken the final constraints on the planet population. It simply contributes less to the constraints than the other stars. The available information is used optimally and correctly, and does not under- or over-constrain the final results.

We can easily appreciate the utility of this method if we consider the example of a star with only very bright candidates detected at large physical separations. Suppose these candidates are too bright to be planets or are detected beyond 500 AU from the primary. Then the planet population constraints on this system (inside 500 AU, if the detections were outside) are just as strong as they would be if there were no detections. Another advantage of this method is that population constraints can be calculated in the middle of the survey, even before any planet candidates are re-observed to check for common proper-motion.

The total likelihood is the product of the detection likelihoods calculated for the individual bins. We chose bin widths in ΔH of 2 mags, with bins from 5 to 23 mags. We chose ρ bins with inner edges from 0.36'' to 9.8'' (outer edges from 0.54'' to 14.8''). The innermost bin is given a width of 0.18'' and each subsequent bin is larger by factor of 1.5. Thus, we are using both astrometric and photometric information from any detected planets and the detection multiplicity information for each system to calculate our constraints.

To demonstrate the validity of our Bayesian approach, we simulate the planet detections from a fictitious planet population with $\alpha = -1.1$, $\beta = -0.6$, $a_{max} = 193$ AU (corresponding to one a_{max} bin), and average planet multiplicity $F = 3$, around our survey stars and assume the survey contrast curves. This fictitious population creates dozens of planet detections for our survey. We compute the likelihoods for values of α and β between -2.5 and $+2.5$, dividing the range into 50 equal-sized bins. For a_{max} , we use 50 values between 20 and 1000 AU, spaced logarithmically. For F , we use 100 values between 0.005 and 20, spaced logarithmically. The resulting probability distributions are shown in Figure 14. The resulting 2σ limits for the parameters are consistent with the simulation input values, and show that our method is effective at narrowing the range of possible planet populations. The 1σ limits

are also consistent with the simulation input values, yielding constraints: $\alpha = [-1.35, -0.85]$, $\beta = [-0.85, -0.2]$, $a_{max} = [153, 193]$ AU and $F = [1.6, 3.2]$. However, the limits also show that even if we had dozens of detections, we would only be able to set moderately stringent constraints on the debris disk planet population, because of the sensitivity limits and the size of our sample of target stars.

We now have the tools to include in our analysis the HR 8799 bcd planet detections and their astrometry and photometry ($\rho = 1.72''$, $0.96''$, $0.61''$ and $\Delta H = 12.6$, 11.6 , 11.6 mag respectively) from the Vigan et al. (2012) survey of A and F stars. We thus expand our sample to include the contrast curves from the six debris disk stars that were in the Vigan survey but not in ours: HR 8799, HIP 22192, HIP 10670, HIP 26309, HIP 69732, HIP 41152 (only HR 8799 had planet detections). We also include the Bonnefoy et al. (2013) detection of β Pictoris b ($\rho \sim 0.5''$, $\Delta H \sim 10$ mag).

Figure 15 shows the Bayesian constraints calculated for our augmented NICI debris disk survey. Since the 2σ limits show a correlation between α and β , and also β and a_{max} , we quote the constraints as follows. Either $\beta < -0.8$ or both $\alpha > 1.7$ and $a_{max} < 200$ AU. The planet frequency is forced to rise sharply with mass ($\alpha > 1.7$), because all our detected planets have masses above $5M_{Jup}$, even though lower masses could easily have been detected at these separations. Either the steep β (< -0.8), or the small a_{max} (< 200 AU) prevents planets from appearing at larger separations. Additionally, we see that many planets (but < 12) are allowed around most stars, since most of them are placed within 10 AU where the survey sensitivity is poor (see Figure 13.) However, as we see next, many fewer planets are allowed at larger SMA.

The upper limits on the number of planets for different planet mass and SMA ranges can now be calculated from the 4-dimensional probability density function of α , β , a_{max} and F_p . For each mass and SMA bin (3-6 M_{Jup} and 25–125 AU, for example), we calculate the number of planets predicted by each model in the 4D function. Thus in each bin, we have a range of predicted planet counts and the associated probability for each total count. From this new probability density function, we calculate 95% upper limits on the number of planets in each bin. The number of stars with at least one planet is calculated from the planet multiplicity using their Poisson relation as done in § 4.5.2. The results are shown in Tables 9 and 10. Notably, $< 21\%$ of stars are allowed to have a $\geq 3M_{Jup}$ planet outside of 40 AU, while $< 13\%$ of stars are allowed to have a $\geq 5M_{Jup}$ planet outside of 80 AU at 95% confidence level. Unlike Figure 13, which shows the model-independent upper limits to planet frequencies, Tables 9 and 10 are consistent with the planet mass and SMA power-law models. Because of the HR 8799 planets, the mass distribution is forced to rise at higher masses ($\alpha > 1.7$), and at small separations the upper limits are nearly constant across the

mass bins. There is of course a caveat to these results: they simply represent the best models out of the ones we compared to the data, and it is quite possible that power-law distributions cannot describe the true planet population. We should also remember that (1) our models do not produce companion masses above $13 M_{Jup}$, and (2) only models with α and β between -2.5 to 2.5, and a_{max} between 20 and 1000 AU were compared to the data.

The β Pic and HR 8799 planets could in principle belong to a small distinct sub-population of massive planets separate from the true tail of the planet distribution beyond 10 AU. Thus, we also calculate population constraints without including these planets (Figure 16). In this case, the 2σ constraints imply that either $\beta < -0.8$ or both $\alpha < -1.5$ and $a_{max} < 125$ AU. We also calculate the upper limits to the planet frequencies as a function of mass and SMA (Tables 11 and 12). Notably, $<20\%$ of stars are allowed to have a $\geq 3M_{Jup}$ planet outside of 10 AU, while $<13\%$ of stars are allowed to have a $\geq 5M_{Jup}$ planet outside of 20 AU.

To investigate the dependence of planet multiplicity on stellar mass, we change the planet-population model so that the multiplicity is given by $F_P = (M_*)^\gamma$, where M_* is the stellar mass. We repeat the Bayesian analysis for the augmented NICI survey (with additions from the Vigan et al. survey). We find that the 1σ limits on γ are $[0.3, 3.2]$, which implies that an A5V star is predicted to have 1.2 to 9.2 times more planets than a G2V star (Figure 17). But given the 2σ limits on γ ($[-0.5, 4.7]$), it is still possible that the planet-frequency does not rise with stellar mass.

5. DISCUSSION

Thus far, observations have only weakly linked debris disks and planet formation. Direct imaging surveys seem to suggest a relatively higher yield of giant planets around A stars with debris disks (i.e. β Pic b and HR 8799 bcde). These detections are consistent with the core-accretion process producing more planets around higher mass stars, which have more massive disks, and also with the extrapolations from the RV planet population (Crepp & Johnson 2011, but see discussion in Nielsen et al. 2013). Gravitational instability models also produce more planets around higher mass stars and moreover are able to produce the HR 8799 planets (Boss 2011) Nero & Bjorkman (2009) found that disk instability models typically require disk masses of 0.03 to $1.3M_\odot$ to produce substellar companions of mass 2 – $21M_{Jup}$ at separations beyond 60 AU, but Boss (2011) has argued that these calculations underestimate the efficiency of the process, because of over-simplified cooling time assumptions.

However, giant planets on very wide (≥ 100 AU) orbits are generally rare, which also

implies that planet formation by core accretion probably dominates over formation by disk instability (Nielsen & Close 2010; Janson et al. 2011). From Figure 13 we see that such companions beyond 60 AU are absent for 90% of debris disk stars, and thus they probably never experienced disk-instability.

Until now, only a weak correlation has been found between debris disks and RV planets (Moro-Martín et al. 2007; Bryden et al. 2009; Lawler & Gladman 2012; Wyatt et al. 2012). No correlation has been found yet between debris disks and stellar metallicity (Beichman et al. 2006), while there is a strong correlation between giant RV planets and metallicity (Fischer & Valenti 2005). However, this correlation weakens significantly for planets smaller than Neptune (Buchhave et al. 2012). Thus it seems that high metallicity is not a requirement for debris disks or for small planets, although we do not know at this time whether the occurrence of the two are correlated. Not finding correlations with debris disks or stellar metallicities increases the probability that small planets are abundant, since debris disks and very high-metallicity stars are rare.

To properly interpret the constraints on the planet population around our target stars, we have to consider the selection effects that went into creating our sample. The NICI Campaign stars were mostly selected by calculating the planet detection probabilities (f_j) for stars which were young or nearby or massive and choosing the highest values (Liu et al. 2010). This sample was then supplemented with interesting stars, such as stars with debris disks.

The sources for the debris disk targets were largely compilations of Moór et al. (2006) and Rhee et al. (2007), which were based on the IRAS all-sky survey and supplemented by the ISO survey. These compilations included stars of spectral types BAFGKM and systems with fractional disk luminosities (L_d/L_*) as low as 10^{-5} . Also included in the Campaign were the most promising stars (based on planet detection probability) of those found to have excess in the A star *Spitzer* surveys of Rieke et al. (2005) and Su et al. (2006) at 24 μm and 70 μm , respectively. These surveys were sensitive to L_d/L_* as low as 10^{-6} , limited by calibration uncertainties at mid- to far-infrared wavelengths, which limit the excess disk emission that can be detected relative to the photospheric emission. Because debris disks are easier to detect around bright stars, our sample is biased towards A stars. *Spitzer* surveys have also been conducted around FGK stars (Meyer et al. 2008), but the most IR-luminous targets from these surveys were already included in the Campaign by drawing from the IRAS and ISO surveys mentioned above. Thus, our debris disk stars are the youngest and nearest of the known debris disks, which are mostly complete to $L_d/L_* = 10^{-5}$.

It is thought that almost no disk with $L_d/L_* < 10^{-2}$ is primordial, as the small dust grains responsible for the excess luminosity are expected to be dispersed on time scales much

shorter than the ages of the debris disk stars (Backman and Paresce 1993). A few debris disks are known to have small amounts of gas, e.g. β Pic and 49 Cet (Brandeker et al. 2004; Dent et al. 2005). However, it is believed that the gas probably has a non-primordial origin like planetesimal collisions or sublimation (Czechowski & Mann 2007; Beust & Valiron 2007; Chen et al. 2007). Thus, all the debris disks in our sample are very likely composed of second-generation dust created by collisions between larger rocky bodies (Backman & Paresce 1993).

There are three main explanations for how the detectable dust in debris disks are produced: (1) steady-state collisions between >1 -100 km size planetesimals (Wyatt & Dent 2002; Quillen et al. 2007) which gradually decrease over hundreds of Myrs (Wyatt et al. 2007; Dominik & Decin 2003); (2) chance, rare collisions between ~ 1500 km protoplanets (Wyatt & Dent 2002), which produce dust that is detectable for a few million years, and (3) the delayed stirring of a planetesimal belt when a large object (≥ 2000 km) is formed (Kenyon & Bromley 2004). Other dust production mechanisms, such as sublimation of comets (Beichman et al. 2005) or planet migration (Gomes et al. 2005) also require already existing massive bodies. Thus, stars with debris disks are different from other young stars in the NICI Campaign, in that they very likely possess >1 -100 km sized planetesimals which are the sources of their dust, and potentially protoplanets and planets which stir the smaller bodies.

The fraction of stars with inner dust disks decrease from $>80\%$ to $<5\%$ from 0.3 to 15 Myrs as seen in surveys of near- to mid-infrared studies of open clusters (Hernández et al. 2007). However, we know that 16% of sun-like stars older than 1 Gyrs possess debris disks (see discussion in Koerner et al. 2010; Trilling et al. 2008). An even larger fraction possess close-in super earth planets (Howard et al. 2010; Wittenmyer et al. 2011; Mayor et al. 2011). For the rest of the stars, it is still possible that the dust has formed into pebbles, planetesimals or protoplanets, as yet not detectable, somewhere in the system.

Observations of stars with transition disks, i.e. primordial disks that have developed inner holes, provide additional statistics on the fraction of stars with planets. All disks are thought to undergo an evolution from an accreting, massive disk phase to gas-poor, low fractional-luminosity debris disks. The evolutionary change may not always be recognizable, but transition disks are thought to be objects from this period. Cieza et al. (2012) found in a study of 34 transition disks that roughly 18% are in a planet-forming phase, 18% are in a grain-growth phase (likely an earlier phase), and 64% are in the debris disk or photo-evaporation phase (likely a later phase). The accreting disks that have rising spectral energy distributions in the mid to far-infrared and but low fluxes in the near to mid-infrared, indicating massive disks with inner holes are very likely to be undergoing planet formation. The sharp inner holes that are necessary to produce the observed SEDs cannot be produced

by alternate explanations, i.e., photo-evaporation and grain growth. Indeed LkCa 15, a star with such a transition disk, was recently found to have a planetary object in formation within its inner cavity (Kraus & Ireland 2012). The results suggest that at least 18% of stars form planets, while it is uncertain whether the stars in the other stages will ever undergo or have already undergone planet formation. However, these planets either have small orbital separations (< 40 AU) or are too small ($< 3 M_{Jup}$) to be detected by our debris disk survey.

Recently, using simulations that examined the survival of debris disks and terrestrial planets in systems with already existing giant planets ($1 M_{sat}$ to $3 M_{Jup}$), Raymond et al. (2011, 2012) predicted that (1) debris disks should be anti-correlated with eccentric giant planets (usually in wide-orbits); (2) disks have a high probability ($\sim 95\%$) of surviving in systems with low-mass giant planets ($\leq 1 M_{Jup}$); and (3) massive outer disks tend to stabilize inner giant planets and also lead to long disk lifetimes. Thus, the massive giant planets on wide orbits that the Campaign is sensitive to may be much less prevalent in our debris disk sample than in other non-debris Campaign stars. At the same time, low-mass giant planets may be more prevalent in the debris disk sample. The Raymond et al. (2012) simulations also suggest that β Pic and HR 8799 were once accompanied by massive outer disks ($\sim 100 M_{\oplus}$), since they both have very massive planets ($5\text{--}10 M_{Jup}$) which probably required a massive disk to stabilize them.

Twenty two of the 57 debris disks in our sample have resolved disks around them and most of these have asymmetries in them in the form of arcs, clumps, etc. Asymmetries are the strongest indicators of the influence of planetary mass objects (Wyatt 2008), although the location of the unseen planets cannot be uniquely determined from them. This may be the most important distinction between debris disk stars and other groups of stars included in the Campaign.

6. CONCLUSIONS

We have completed a direct imaging survey for giant planets around 57 debris disk stars as part of the Gemini NICI Planet-Finding Campaign. We achieved median contrasts at H -band of 12.4 mag at $0.5''$ and 14.1 mag at $1''$. We detected a total of 78 planet candidates around 23 stars. Follow-up observations of 19 targets with 66 of the most promising candidates (projected separation < 500 AU), show that all of them are background objects.

We have developed a more general Bayesian formalism than previous studies, which allowed us to use (1) non-detections, (2) single-epoch detections, and (3) multiple confirmed detections in a single system along with (4) their astrometric and (5) photometric infor-

mation to constrain the planet population. We demonstrated the validity of this approach by simulating an input planet population and recovering good estimates for the population parameters. We also show that the statistical formulation used in Nielsen et al. (2008) and Nielsen & Close (2010) is consistent with our more general Bayesian formulation and we discuss the bounds of the applicability of the earlier method. We also discuss under what assumptions the method presented in Lafrenière et al. (2007) is consistent with ours.

In our new statistical formulation, we make a distinction between the fraction of stars with planets and the average planet multiplicity. We assume a Poisson distribution in planet multiplicity to represent the planet population model, such that the two statistics are naturally related. However, it is also possible to study other population models within our Bayesian formulation. The most interesting aspect of our new formalism is that both astrometric and photometric information about detected planets can be used to constrain the planet population. Also multiple planet detections around a single star, such as in the HR 8799bcde system, can be incorporated into constraint calculations. Thus, the formulation can be naturally applied to the upcoming direct-imaging surveys, SPHERE and GPI, from which multiple planet detections are more feasible.

We used our Bayesian method to analyze the statistical properties of the underlying planet population, based on our contrast curves for all targets (plus 6 extra stars from Vigan et al. 2012.) For this total debris disk sample, we find at the 95% confidence level that <21% of debris disk stars have a $\geq 3M_{Jup}$ planet outside of 40 AU, and <13% of stars have a $\geq 5M_{Jup}$ planet beyond 80 AU. We also find that indeed multiple massive planets per system may still remain undetected by direct-imaging surveys inside of 5 AU. The Bayesian constraints on the planet-mass power-law index (α) and the SMA power-law index (β) show that either $\beta < -0.8$ or both $\alpha > 1.7$ and $a_{max} < 200$ AU, where a_{max} is the maximum allowed SMA. The planet frequency is forced to rise sharply with mass ($\alpha > 1.7$), because all our detected planets have masses above $5M_{Jup}$, even though lower masses could easily have been detected at these separations.

Since, the β Pic and HR 8799 planets may represent a distinct population of massive planets separate from the true tail of the planet-distribution, we also calculated population constraints without including these planets. In this analysis, our 2σ constraints show that either $\beta < -0.8$ or both $\alpha < -1.5$ and $a_{max} < 125$ AU. Also, we found a possible weak correlation between planet-frequency and stellar mass but our 2σ constraints are still consistent with no correlation. We also estimate that <20% of stars are allowed to have a $\geq 3M_{Jup}$ planet outside of 10 AU, while <13% of stars are allowed to have a $\geq 5M_{Jup}$ planet outside of 20 AU. These constraints are stronger than what previous surveys have found because of the improved performance of NICI.

We did not detect the Fomalhaut planet in our NICI observations of the star. With 99% confidence that there are no planets with $CH_4S < 20.0 \pm 0.3$ mag near the location of the Kalas et al. (2008) detection. The upper limit on the mass of the planet from the NICI observations is 12–13 M_{Jup} , assuming thermal emission and an age of 450 ± 40 Myr for Fomalhaut (Mamajek 2012). Thus, it is not surprising that we do not detect the planet.

A study of transition disks (those with inner holes) by Cieza et al. (2012) suggested that roughly 18% are in a planet-forming phase, 18% are in a grain-growth phase (likely an earlier phase), and 64% are in the debris disk or photo-evaporation phase (likely a later phase). This suggests that at least 18% of stars form planets, while it is uncertain whether the other stars will ever undergo or have already undergone planet formation. However, these planets either have small orbital separations (< 40 AU) or are too small ($< 3 M_{Jup}$) to be detected by our debris disk survey.

This work was supported in part by NSF grants AST-0713881 and AST-0709484. The Gemini Observatory is operated by the Association of Universities for Research in Astronomy, Inc., under a cooperative agreement with the NSF on behalf of the Gemini partnership: the National Science Foundation (United States), the Science and Technology Facilities Council (United Kingdom), the National Research Council (Canada), CONICYT (Chile), the Australian Research Council (Australia), CNPq (Brazil), and CONICET (Argentina). Our research has employed the 2MASS data products; NASA’s Astrophysical Data System; the SIMBAD database operated at CDS, Strasbourg, France. We thank Ruobing Dong and Lucas Cieza for discussions on the importance of transition disks to planet formation.

Facilities: Gemini-South (NICI).

A. APPENDIX

Here we present the full derivation of the probability distribution for F , the frequency of planets around single stars.

$$P(F, n \mid \{n_j\}, \{f_j\}, I) = P(\{n_j\}, \{f_j\} \mid F, n, I) \frac{P(F, n \mid I)}{P(\{n_j\}, \{f_j\} \mid I)},$$

We set the denominator on the right side of the equation to 1, because we assume that there is no bias in our sampling of stars, other than that we have chosen young nearby stars with debris disks (we explicitly state that our conclusions are only valid for this sample). Using the notation D_j for n_j, f_j , and assuming that the $\{D_j\}$ are independent

$$\begin{aligned} P(\{D_j\} \mid F, n, I) &= P(D_1 \mid D_{j=2..N}, F, n, I) P(D_{j=2..N} \mid F, n, I) \\ &= \prod_{j=1}^N P(D_j \mid F, n, I) = \prod_{j=1}^N P(n_j, f_j \mid F, n, I) \\ &= \prod_{j=1}^N P(n_j \mid f_j, F, n, I) P(f_j \mid F, n, I) = \prod_{j=1}^N P(n_j \mid f_j, F, n, I), \end{aligned}$$

since $P(f_j \mid F, n, I) = 1$ as the f_j s only depend on the contrasts achieved and the power-law behavior of the population model and not on the overall normalization. Also, we have

$$P(F, n \mid I) = P(n \mid F, I) P(F \mid I) = P(n \mid F, I),$$

since we assume that there is no prior information on the frequency of planets and thus set $P(F \mid I) = 1$. Thus, we have (since $P(n_j \mid f_j, F, n, I) = P(n_j \mid f_j, n, I)$)

$$P(F, n \mid \{n_j\}, \{f_j\}, I) = \prod_{j=1}^N P(n_j \mid f_j, n, I) P(n \mid F, I).$$

Finally, summing over the nuisance parameter n , we have the probability distribution for the frequency of planets as presented in § 4.5.1:

$$P(F \mid \{n_j\}, \{f_j\}, I) = \prod_{j=1}^N \left(\sum_n P(n_j \mid f_j, n, I) P(n \mid F, I) \right).$$

B. APPENDIX

Lafrenière et al. (2007) used the following expression for the likelihood of F_{sp} (in our notation):

$$P(d_j | F_{sp}, I) = \prod_{j=1}^N (F_{sp} f_j)^{d_j} (1 - F_{sp} f_j)^{1-d_j}, \quad (\text{B1})$$

where $d_j = 0$ if no planets are detected around star j , and $d_j = 1$ otherwise. The likelihood that the star has one or more planets is written as $F_{sp} f_j$. In other words, in this model, every star has exactly F_{sp} planets within the chosen mass and SMA range, and thus it is not possible to accommodate stars with 0 planets and stars with ≥ 4 planets (e.g. HR 8799) within the same population model.

The other limitation of this formulation is that all systems with non-zero detections are considered the same. Thus, we are throwing away information and the constraints on the model are not optimum given the data.

To examine the special case where our formulations agree, let us force a simpler model where a star can have exactly 1 or 0 planets (similar to Nielsen et al. 2008), even though the model will not be able to describe real data sets with multiple planet discoveries. Thus, $F = F_{sp} * 1 + (1 - F_{sp}) * 0 = F_{sp}$. Also, let us set the probabilities to $P(1 | F) = F$ and $P(0 | F) = 1 - F$, instead of using the Poisson likelihoods. Similarly, let us replace $P(1 | f_j) = f_j$ and $P(0 | f_j) = 1 - f_j$. Then, using our Bayesian result from earlier and summing over $n = \{0, 1\}$, we get

$$\begin{aligned} P(F | n_j = 0, 1, f_j, I) &= \prod_{j=1}^N \left(P(n_j | 0) P(0 | F) + P(n_j | 1 f_j) P(1 | F) \right) \\ &= \prod_{j=1}^N \left(P(n_j | 0) (1 - F) + P(n_j | f_j) F \right) \\ &= \prod_{j=1}^N \left(P(1 | 0) (1 - F) + P(1 | f_j) F \right)^{n_j} \left(P(0 | 0) (1 - F) + P(0 | f_j) F \right)^{1-n_j} \\ &= \prod_{j=1}^N \left(f_j F \right)^{n_j} \left((1 - F) + (1 - f_j) F \right)^{1-n_j} \\ &= \prod_{j=1}^N (f_j F)^{n_j} (1 - f_j F)^{1-n_j}. \end{aligned}$$

This is the same expression as in Lafrenière et al. (2007). Thus their approach agrees with ours for small F and when a star can only have 1 or 0 planets.

For multiple planet systems, we can generalize the expression of Lafrenière et al. (2007) to

$$P(\text{data}|\text{model}, I) = P(\{d_{jk}\}|\{F_{nk}\}) = \prod_j \prod_k \sum_n F_{nk}^{d_{jk}},$$

where F_{nk} is the probability of k planet detections in systems with n planets, and d_{jk} is 1 if k planets are detected around star j and 0 otherwise. Since the number of actual planets in a system can vary, we sum over n thus marginalizing over this parameter. Now, we make the following expansion:

$$\begin{aligned} F_{nk} &= (\text{probability that } n \text{ planets exist in system } j) \\ &\times (\text{probability that } k \text{ planets will be detected given the contrast limits}) \\ &= P(n | F) P(k_j | n f_j) \end{aligned}$$

This expression is the same as our result in Eq. 5.

REFERENCES

- Backman, D. E., & Paresce, F. 1993, in Protostars and Planets III, ed. E. H. Levy & J. I. Lunine, 1253–1304
- Baraffe, I., Chabrier, G., Allard, F., & Hauschildt, P. 2003a, in IAU Symposium, Vol. 211, Brown Dwarfs, ed. E. Martín, 41
- Baraffe, I., Chabrier, G., Barman, T. S., Allard, F., & Hauschildt, P. H. 2003b, A&A, 402, 701
- Beichman, C. A., et al. 2005, ApJ, 626, 1061
- . 2006, ApJ, 652, 1674
- Beust, H., & Valiron, P. 2007, A&A, 466, 201
- Biller, B. A., et al. 2007, ApJS, 173, 143
- Bonnefoy, M., et al. 2013, ArXiv e-prints
- Boss, A. P. 2011, ApJ, 731, 74

- Brandeker, A., Liseau, R., Olofsson, G., & Fridlund, M. 2004, *A&A*, 413, 681
- Bryden, G., et al. 2009, *ApJ*, 705, 1226
- Buchhave, L. A., et al. 2012, *Nature*, 486, 375
- Chen, C. H., et al. 2006, *ApJS*, 166, 351
- . 2007, *ApJ*, 666, 466
- Cieza, L. A., Schreiber, M. R., Romero, G. A., Williams, J. P., Rebassa-Mansergas, A., & Merín, B. 2012, *ApJ*, 750, 157
- Crepp, J. R., & Johnson, J. A. 2011, *ApJ*, 733, 126
- Cumming, A., Butler, R. P., Marcy, G. W., Vogt, S. S., Wright, J. T., & Fischer, D. A. 2008, *PASP*, 120, 531
- Currie, T., et al. 2012, *ApJ*, 760, L32
- Czechowski, A., & Mann, I. 2007, *ApJ*, 660, 1541
- Dent, W. R. F., Greaves, J. S., & Coulson, I. M. 2005, *MNRAS*, 359, 663
- Dominik, C., & Decin, G. 2003, *ApJ*, 598, 626
- Fabrycky, D. C., & Murray-Clay, R. A. 2010, *ApJ*, 710, 1408
- Fischer, D. A., & Valenti, J. 2005, *ApJ*, 622, 1102
- Fortney, J. J., Marley, M. S., Saumon, D., & Lodders, K. 2008, *ApJ*, 683, 1104
- Galicher, R., Marois, C., Zuckerman, B., & Macintosh, B. 2013, *ApJ*, 769, 42
- Gomes, R., Levison, H. F., Tsiganis, K., & Morbidelli, A. 2005, *Nature*, 435, 466
- Gray, R. O., Corbally, C. J., Garrison, R. F., McFadden, M. T., Bubar, E. J., McGahee, C. E., O’Donoghue, A. A., & Knox, E. R. 2006, *AJ*, 132, 161
- Gray, R. O., Corbally, C. J., Garrison, R. F., McFadden, M. T., & Robinson, P. E. 2003, *AJ*, 126, 2048
- Henry, T. J., Soderblom, D. R., Donahue, R. A., & Baliunas, S. L. 1996, *AJ*, 111, 439
- Hernández, J., et al. 2007, *ApJ*, 662, 1067

- Hillenbrand, L. A., et al. 2008, *ApJ*, 677, 630
- Howard, A. W., et al. 2010, *Science*, 330, 653
- . 2012, *ApJS*, 201, 15
- Janson, M., Bonavita, M., Klahr, H., Lafrenière, D., Jayawardhana, R., & Zinnecker, H. 2011, *ApJ*, 736, 89
- Janson, M., Carson, J. C., Lafrenière, D., Spiegel, D. S., Bent, J. R., & Wong, P. 2012, *ApJ*, 747, 116
- Jenkins, J. S., Jones, H. R. A., Pavlenko, Y., Pinfield, D. J., Barnes, J. R., & Lyubchik, Y. 2008, *A&A*, 485, 571
- Jenkins, J. S., et al. 2006, *MNRAS*, 372, 163
- Kalas, P., et al. 2008, *Science*, 322, 1345
- Kenyon, S. J., & Bromley, B. C. 2004, *AJ*, 127, 513
- Kenyon, S. J., & Hartmann, L. 1995, *ApJS*, 101, 117
- Koerner, D. W., et al. 2010, *ApJ*, 710, L26
- Kraus, A. L., & Ireland, M. J. 2012, *ApJ*, 745, 5
- Kuchner, M. J., & Holman, M. J. 2003, *ApJ*, 588, 1110
- Lafrenière, D., et al. 2007, *ApJ*, 670, 1367
- Lagrange, A., et al. 2009, *A&A*, 493, L21
- Lawler, S. M., & Gladman, B. 2012, *ApJ*, 752, 53
- Leconte, J., et al. 2010, *ApJ*, 716, 1551
- Liu, M. C., et al. 2010, in *Society of Photo-Optical Instrumentation Engineers (SPIE) Conference Series*, Vol. 7736, *Society of Photo-Optical Instrumentation Engineers (SPIE) Conference Series*
- Low, F. J., Smith, P. S., Werner, M., Chen, C., Krause, V., Jura, M., & Hines, D. C. 2005, *ApJ*, 631, 1170
- Mamajek, E. E. 2012, *ApJ*, 754, L20

- Marois, C., Macintosh, B., Barman, T., Zuckerman, B., Song, I., Patience, J., Lafrenière, D., & Doyon, R. 2008, *Science*, 322, 1348
- Martínez-Arnáiz, R., Maldonado, J., Montes, D., Eiroa, C., & Montesinos, B. 2010, *A&A*, 520, A79
- Mayor, M., et al. 2011, ArXiv e-prints
- Meyer, M. R., et al. 2008, *ApJ*, 673, L181
- Moór, A., Ábrahám, P., Derekas, A., Kiss, C., Kiss, L. L., Apai, D., Grady, C., & Henning, T. 2006, *ApJ*, 644, 525
- Morales, F. Y., Rieke, G. H., Werner, M. W., Bryden, G., Stapelfeldt, K. R., & Su, K. Y. L. 2011, *ApJ*, 730, L29
- Moro-Martín, A., et al. 2007, *ApJ*, 658, 1312
- Nero, D., & Bjorkman, J. E. 2009, *ApJ*, 702, L163
- Nielsen, E. L., & Close, L. M. 2010, *ApJ*, 717, 878
- Nielsen, E. L., Close, L. M., Biller, B. A., Masciadri, E., & Lenzen, R. 2008, *ApJ*, 674, 466
- Ozernoy, L. M., Gorkavyi, N. N., Mather, J. C., & Taidakova, T. A. 2000, *ApJ*, 537, L147
- Quanz, S. P., Crepp, J. R., Janson, M., Avenhaus, H., Meyer, M. R., & Hillenbrand, L. A. 2012, *ApJ*, 754, 127
- Quillen, A. C., Morbidelli, A., & Moore, A. 2007, *MNRAS*, 380, 1642
- Raymond, S. N., et al. 2011, *A&A*, 530, A62
- . 2012, *A&A*, 541, A11
- Rebull, L. M., et al. 2008, *ApJ*, 681, 1484
- Rhee, J. H., Song, I., Zuckerman, B., & McElwain, M. 2007, *ApJ*, 660, 1556
- Rieke, G. H., et al. 2005, *ApJ*, 620, 1010
- Smith, B. A., & Terrile, R. J. 1984, *Science*, 226, 1421
- Su, K. Y. L., et al. 2006, *ApJ*, 653, 675
- Trilling, D. E., et al. 2008, *ApJ*, 674, 1086

- van Leeuwen, F. 2007, *A&A*, 474, 653
- Vigan, A., et al. 2012, ArXiv e-prints
- Wahhaj, Z., Koerner, D. W., & Sargent, A. I. 2007, *ApJ*, 661, 368
- Wahhaj, Z., et al. 2011, *ApJ*, 729, 139
- Wittenmyer, R. A., Tinney, C. G., Butler, R. P., O’Toole, S. J., Jones, H. R. A., Carter, B. D., Bailey, J., & Horner, J. 2011, *ApJ*, 738, 81
- Wright, J. T., Marcy, G. W., Butler, R. P., & Vogt, S. S. 2004, *ApJS*, 152, 261
- Wyatt, M. C. 2008, *ARA&A*, 46, 339
- Wyatt, M. C., & Dent, W. R. F. 2002, *MNRAS*, 334, 589
- Wyatt, M. C., Smith, R., Su, K. Y. L., Rieke, G. H., Greaves, J. S., Beichman, C. A., & Bryden, G. 2007, *ApJ*, 663, 365
- Wyatt, M. C., et al. 2012, ArXiv e-prints
- Zuckerman, B. 2001, *ARA&A*, 39, 549
- Zuckerman, B., Rhee, J. H., Song, I., & Bessell, M. S. 2011, *ApJ*, 732, 61
- Zuckerman, B., & Song, I. 2004, *ARA&A*, 42, 685

Table 1. Debris Disk Stars Observed by the NICI Campaign.

Target	R.A.	Dec.	Dist. (pc)	Sp. Type	Age* (Myr)	V (mag)	H (mag)	K (mag)
HR 9	00:06:50	−23:06:27	39.1	F2	12 ¹	6.20	5.33	5.24
HIP 1481	00:18:26	−63:28:39	41.0	F9	30 ¹	7.46	6.25	6.09
49 Cet	01:34:37	−15:40:34	61.0	A1	40 ¹⁰	5.62	5.53	5.46
HD 10472	01:40:24	−60:59:56	67.0	F2	30 ¹	7.62	6.69	6.63
HD 10939	01:46:06	−53:31:19	57.0	A1	346 ²	5.00	5.03	4.96
HIP 10679	02:17:24	+28:44:31	34.0	G2	12 ¹	7.80	6.36	6.26
HD 15115	02:26:16	+06:17:33	45.0	F4	12 ¹	6.79	5.81	5.77
HD 17848	02:49:01	−62:48:23	50.7	A2	372 ²	5.30	5.16	4.97
HD 19668	03:09:42	−09:34:46	40.2	G0	100 ¹⁰	8.48	6.79	6.70
HD 21997	03:31:53	−25:36:51	74.0	A3	225 ³	6.38	6.11	6.10
ϵ Eri	03:32:55	−09:27:29	3.2	K2	1129 ⁴	3.73	1.88	1.51
HD 24966	03:56:29	−38:57:43	104.0	A0	128 ¹⁰	6.89	6.87	6.86
HD 25457	04:02:36	−00:16:08	19.2	F5	100 ¹⁰	5.38	4.34	4.28
HD 27290	04:16:01	−51:29:12	20.3	F4	300 ²	4.30	3.47	3.51
HD 31295	04:54:53	+10:09:03	37.0	A0	241 ²	4.60	4.52	4.42
HD 32297	05:02:27	+07:27:39	112.0	A0	224 ¹	8.13	7.62	7.59
HIP 25486	05:27:04	−11:54:04	26.8	F7	12 ¹	6.30	5.09	4.93
HD 37484	05:37:39	−28:37:34	60.0	F3	30 ¹⁰	7.26	6.29	6.28
HD 38207	05:43:20	−20:11:21	103.0	F2	20 ⁵	8.47	7.55	7.49
HD 38206	05:43:21	−18:33:26	69.0	A0	30 ²	5.73	5.84	5.78
ζ Lep	05:46:57	−14:49:18	22.0	A2	12 ¹³	3.55	3.31	3.29
β Pic	05:47:17	−51:03:59	19.3	A5	12 ¹	3.90	3.54	3.53
HD 40136	05:56:24	−14:10:03	15.0	F1	300 ²	3.70	2.98	2.99
HD 53143	06:59:59	−61:20:10	18.0	K0	300 ²	6.81	5.10	4.99
HD 54341	07:06:20	−43:36:38	93.0	A0	154 ¹⁰	6.52	6.48	6.48
HD 61005	07:35:47	−32:12:14	34.5	G3	100 ²	8.20	6.58	6.46
HD 71155	08:25:39	−03:54:23	38.3	A0	276 ¹⁰	3.90	4.09	4.08
HD 85672	09:53:59	+27:41:43	93.0	A0	205 ¹⁰	7.59	7.20	7.19
TWA 7	10:42:30	−33:40:16	28.0	M2	10 ⁷	11.65	7.74	7.54
TW Hya	11:01:52	−34:42:17	56.4	K7	10 ⁷	10.80	7.56	7.30
TWA 13A	11:21:17	−34:46:46	55.0	M1	10 ⁷	11.46	7.77	7.59
TWA 13B	11:21:17	−34:46:50	55.0	M1	10 ⁷	11.96	8.27	8.09
HD 102647	11:49:03	+14:34:19	11.1	A3	215 ¹⁰	2.10	1.92	1.88
HD 107146	12:19:06	+16:32:53	28.5	G2	185 ⁵	7.07	5.61	5.61
HD 109085	12:32:04	−16:11:45	18.2	F2	100 ²	4.31	3.37	3.46
HR 4796 A	12:36:01	−39:52:10	67.1	A0	10 ²	5.80	5.79	5.77
HD 110058	12:39:46	−49:11:55	100.0	A0	50 ²	7.99	7.59	7.58
HD 110411	12:41:53	+10:14:08	36.9	A0	90 ¹³	4.90	4.76	4.68
HD 131835	14:56:54	−35:41:43	111.0	A2	368 ¹⁰	7.88	7.56	7.52
HD 138965	15:40:11	−70:13:40	77.3	A5	157 ¹⁰	6.40	6.34	6.27
HD 139664	15:41:11	−44:39:40	17.5	F5	200 ²	4.64	3.73	3.80
HD 141569	15:49:57	−03:55:16	99.0	B9	5 ²	7.10	6.86	6.82
HD 157728	17:24:06	+22:57:37	43.0	F0	100 ⁵	5.70	5.22	5.18
HIP 85340	17:26:22	−24:10:31	25.7	A3	894 ¹⁰	4.16	3.96	3.95
γ Oph	17:47:53	+02:42:26	29.1	A0	342 ¹⁰	3.70	3.66	3.62
HD 170773	18:33:00	−39:53:31	36.0	F5	200 ²	6.22	5.28	5.20

Table 1—Continued

Target	R.A.	Dec.	Dist. (pc)	Sp. Type	Age* (Myr)	V (mag)	H (mag)	K (mag)
HD 172555 A	18:45:26	−64:52:16	29.2	A5	12 ¹	4.80	4.25	4.42
HD 176638	19:03:06	−42:05:42	56.3	A0	248 ¹⁰	4.70	4.96	4.75
HR 7329	19:22:51	−54:25:24	47.7	A0	12 ¹	5.10	5.15	5.01
HIP 95270	19:22:58	−54:32:15	50.6	F5	12 ¹	7.00	5.98	5.91
HD 182681	19:26:56	−29:44:35	69.0	B8	144 ¹⁰	5.66	5.66	5.68
HD 191089	20:09:05	−26:13:27	53.0	F5	12 ¹	7.18	6.12	6.08
HD 192758	20:18:15	−42:51:36	62.0	F0	40 ⁵	7.02	6.30	6.21
HD 196544	20:37:49	+11:22:39	54.3	A2	272 ¹⁰	5.40	5.37	5.30
GJ 803	20:45:09	−31:20:27	9.9	M0	12 ¹	8.81	4.83	5.16
HD 206893	21:45:21	−12:47:00	39.0	F5	200 ⁵	6.69	5.69	5.59
Fomalhaut	22:57:39	−29:37:19	7.7	A3	450 ⁸	1.20	0.94	0.94

Note. — Age references*: (1) Zuckerman & Song (2004) (2) Rhee et al. (2007) (3) Zuckerman et al. (2011) (4) Nielsen & Close (2010) (5) Moór et al. (2006) (5) Morales et al. (2011) (6) Rieke et al. (2005) (7) Low et al. (2005) (8) Mamajek (2012) (9) Chen et al. (2006) (10) Nielsen et al. 2013

Table 2. Observation of Campaign Debris-Disk Targets

Target	Date	Obs Mode	Number of Images	Total Exp. Time (s)	Total Rotation (deg)
HR 9	2009-12-05	ADI	20	1208	2.8
HR 9	2009-12-05	ASDI	45	2736	22.8
49 Cet	2009-12-02	ASDI	45	2736	40.6
49 Cet	2009-12-02	ADI	20	1208	16.4
HD 10939	2010-12-26	ASDI	44	2708	3.5
HIP 10679	2011-10-16	ASDI	45	2701	13.3
HD 15115	2009-12-04	ADI	20	1208	6.2
HD 15115	2009-12-04	ASDI	43	2598	17.4
HD 15115	2011-11-07	ADI	20	1185	8.6
HD 15115	2011-11-22	ADI	40	2371	13.7
HD 17848	2008-12-16	ADI	20	1200	9.7
HD 17848	2008-12-16	ASDI	45	2650	22.3
HD 19668	2010-08-29	ADI	20	1208	9.1
HD 19668	2010-08-29	ASDI	45	2701	30.6
HD 21997	2009-01-16	ASDI	45	2530	55.6
HD 21997	2009-01-16	ADI	20	1208	3.6
HD 21997	2010-01-09	ADI	20	1208	0.8
HD 21997	2010-10-31	ASDI	50	3021	89.2
HD 21997	2010-12-25	ASDI	27	1631	233.9
ϵ Eri	2009-12-03	ADI	60	3556	18.6
ϵ Eri	2009-12-03	ASDI	60	3556	18.5
ϵ Eri	2011-10-16	ASDI	180	3693	55.7
ϵ Eri	2011-10-16	ASDI	180	3693	55.8
ϵ Eri	2011-10-16	ASDI	180	3693	1.9
HD 24966	2009-01-15	ADI	20	1208	17.1
HD 24966	2009-01-15	ASDI	48	2699	72.3
HD 25457	2009-01-13	ASDI	44	2489	25.5
HD 25457	2009-01-13	ADI	20	1208	8.5
HD 27290	2008-12-18	ADI	20	1185	13.3
HD 27290	2008-12-18	ASDI	45	2565	37.0
HD 27290	2010-01-05	ADI	45	2667	14.5
HD 31295	2009-01-14	ASDI	45	2616	16.4
HD 31295	2009-01-14	ADI	20	1208	8.0
HD 32297	2008-12-17	ADI	20	1200	4.5
HD 32297	2008-12-17	ASDI	45	2701	14.1
HIP 25486	2009-01-14	ASDI	45	2479	34.6
HIP 25486	2009-01-14	ADI	20	1208	12.5
HD 37484	2010-10-31	ASDI	45	2701	195.2
HD 38207	2009-03-10	ASDI	45	2701	15.9
HD 38206	2008-12-18	ADI	20	1200	5.2
HD 38206	2008-12-18	ASDI	50	2964	41.2
ζ Lep	2008-12-15	ADI	20	1200	29.4
ζ Lep	2008-12-15	ASDI	40	2432	34.3
β Pic	2009-12-03	ASDI	131	7964	66.8
β Pic	2009-12-02	ADI	146	8654	72.7

Table 2—Continued

Target	Date	Obs Mode	Number of Images	Total Exp. Time (s)	Total Rotation (deg)
HD 40136	2009-02-09	ASDI	58	3331	86.2
HD 40136	2009-02-11	ADI	20	1208	4.5
HD 53143	2009-01-13	ADI	20	1208	9.8
HD 53143	2009-01-13	ASDI	45	2479	19.9
HD 53143	2010-01-05	ADI	20	1208	8.5
HD 54341	2008-12-15	ADI	20	1200	17.0
HD 54341	2008-12-15	ASDI	44	2641	48.0
HD 61005	2009-01-13	ASDI	80	3435	148.4
HD 61005	2011-04-24	ADI	20	1208	3.5
HD 71155	2008-12-16	ADI	20	1200	15.5
HD 71155	2008-12-16	ASDI	46	2691	20.2
HD 71155	2011-05-14	ADI	20	1200	3.5
HD 85672	2009-01-13	ADI	20	1208	5.7
HD 85672	2009-01-13	ASDI	45	2701	13.7
TWA 7	2009-02-09	ASDI	66	3962	125.3
TWA 7	2009-02-11	ADI	20	1208	2.2
TWA 7	2010-02-28	ADI	20	1208	12.0
TW Hya	2009-02-12	ADI	40	2416	6.3
TW Hya	2009-02-12	ASDI	100	6004	100.7
TWA 13A	2009-03-10	ADI	20	1208	3.4
TWA 13A	2009-03-10	ASDI	45	2701	13.1
TWA 13B	2009-03-11	ASDI	45	2701	14.3
HD 102647	2009-01-18	ASDI	37	2109	15.1
HD 102647	2009-01-18	ADI	20	1185	6.9
HD 107146	2009-01-13	ASDI	75	3933	22.9
HD 107146	2009-01-13	ADI	20	1208	5.2
HD 107146	2010-04-08	ADI	25	1510	8.1
HD 109085	2009-02-06	ASDI	45	2817	46.9
HD 109085	2009-02-06	ADI	20	1208	18.9
HR 4796A	2009-01-14	ASDI	45	2821	25.2
HR 4796A	2009-01-14	ADI	20	1208	21.8
HR 4796A	2012-04-06	ADI	64	3793	82.4
HD 110058	2009-01-17	ADI	20	1208	14.8
HD 110058	2009-01-17	ASDI	45	2701	26.1
HD 110058	2012-03-28	ADI	20	1208	15.0
HD 110411	2009-02-07	ASDI	45	2513	16.8
HD 110411	2009-02-07	ADI	20	1208	7.5
HD 131835	2009-02-12	ASDI	52	3122	35.0
HD 131835	2009-04-10	ADI	45	2718	9.1
HD 138965	2009-02-12	ASDI	68	4702	31.5
HD 139664	2009-02-06	ASDI	42	2633	17.0
HD 139664	2010-05-08	ASDI	46	2884	7.9
HD 139664	2010-05-09	ADI	20	1208	14.3
HD 141569	2009-03-07	ADI	20	1208	10.6
HD 141569	2009-03-07	ASDI	65	3902	25.1

Table 2—Continued

Target	Date	Obs Mode	Number of Images	Total Exp. Time (s)	Total Rotation (deg)
HD 141569	2010-04-08	ASDI	45	2701	23.6
HD 141569	2011-05-03	ASDI	114	6844	58.7
HD 157728	2011-05-16	ADI	20	1208	6.3
HD 157728	2011-05-16	ASDI	45	2736	14.1
HIP 85340	2009-04-13	ASDI	50	3040	319.7
γ Oph	2009-04-08	ASDI	45	2736	20.0
γ Oph	2009-04-08	ADI	20	1185	5.9
γ Oph	2010-04-08	ADI	20	1185	6.4
HD 170773	2011-05-12	ASDI	44	2675	5.0
HD 170773	2011-10-16	ADI	20	1208	4.9
HD 170773	2012-04-06	ADI	20	1208	3.4
HD 172555	2009-04-09	ADI	20	1208	6.8
HD 172555	2009-04-09	ASDI	47	2786	22.0
HD 176638	2011-05-12	ASDI	45	2667	32.4
HD 176638	2011-10-17	ADI	16	966	4.6
HD 176638	2012-04-06	ADI	20	1208	3.9
HR 7329	2009-04-11	ADI	20	1208	8.1
HR 7329	2009-04-11	ASDI	45	2565	22.4
HIP 95270	2009-04-13	ADI	20	1208	7.9
HIP 95270	2009-04-13	ASDI	44	2658	29.2
HD 182681	2010-08-29	ADI	20	1208	3.3
HD 191089	2010-05-11	ASDI	45	2718	311.3
HD 191089	2010-05-11	ADI	20	1208	73.1
HD 192758	2011-05-12	ASDI	45	2667	25.5
HD 196544	2009-04-26	ADI	20	1208	5.0
HD 196544	2009-04-27	ASDI	65	3952	5.2
HD 196544	2010-10-31	ASDI	20	1216	5.4
HD 196544	2011-04-25	ADI	30	1812	9.9
GJ 803	2010-05-09	ASDI	59	3609	60.4
GJ 803	2010-08-28	ADI	53	3021	36.9
HD 206893	2011-10-30	ADI	40	2416	32.9
Fomalhaut	2008-11-17	ASDI	77	5149	6.3
Fomalhaut	2009-12-04	ASDI	99	5868	7.0
Fomalhaut	2009-12-04	ADI	99	5868	6.9
Fomalhaut	2011-10-17	ASDI	80	4864	181.9

Table 3. Properties of Star and Disk

Target	Assoc.	L_d/L_* $\times 10^{-5}$	ref.	Disk Size AU	ref.	Disk Inc. degree	Disk PA degree	ref.
HR 9	BPMG	10	1	200	1	-	-	
HIP 1481	THMG	7.1	3			-	-	
49 Cet	-	92	4	900	2	60	125	2
HD 10472	THMG	67	1	700	1	-	-	
HD 10939	-	6.8	5			-	-	
HIP 10679	BPMG	80	1	200	1	-	-	
HD 15115	BPMG	49	4	872	2	90	278.5	2
HD 17848	-	6.4	7			-	-	
HD 19668	ABDMG	9.9	3			-	-	
HD 21997	THMG	57.6	3			-	-	
ϵ Eri	-	8.3	7	212	2	25	89	2
HD 24966	ABDMG	10	4			-	-	
HD 25457	ABDMG	11	3			-	-	
HD 27290	-	2.3	7			-	-	
HD 31295	-	4.5	6			-	-	
HD 32297	-	334	4	655	2	79	237	2
HIP 25486	BPMG	3	1	200	1	-	-	
HD 37484	THMG	32.5	3			-	-	
HD 38207	GAYA2	108	4			-	-	
HD 38206	THMG	19.1	3			-	-	
ζ Lep	Castor	11	4	6	2	30	50	2
β Pic	BPMG	180	1	501	2	90	32	2
HD 40136	-	2	7			-	-	
HD 53143	-	20	7	110	2	45	147	2
HD 54341	-	20	7			-	-	
HD 61005	-	258	7	207	2	80	70	2
HD 71155	-	2.5	6	3	2	30	140	2
HD 85672	-	49	4			-	-	
TWA 7	TWA	200	9			-	-	
TW Hya	TWA	27000	9	448	2	-	-	2
TWA 13A	TWA	86	9			-	-	
TWA 13B	TWA	89	9			-	-	
HD 102647	-	2	6	78	2	30	125	2
HD 107146	-	92	4	399	2	25	148	2
HD 109085	-	12	7	205	2	45	130	2
HR 4796	-	443	7	140	2	73	27	2
HD 110058	-	254	7			-	-	
HD 110411	-	3.7	6			-	-	
HD 131835	UCL	199	4			-	-	
HD 138965	-	11.7	7			-	-	
HD 139664	-	11.5	7	210	2	87	77	2
HD 141569	-	1120	7	743	2	59	356	2
HD 157728	-	29	4			-	-	
HIP 85340	-	6.7	10			-	-	
γ Oph	-	7.8	7	1047	2	50	55	2

Table 3—Continued

Target	Assoc.	L_d/L_* $\times 10^{-5}$	ref.	Disk Size AU	ref.	Disk Inc. degree	Disk PA degree	ref.
HD 170773	-	46	7			-	-	
HD 172555	BPMG	90	1	200	1	-	-	
HD 176638	-	9.7	7			-	-	
HR 7329	BPMG	24	1	200	1	-	-	2
HIP 95270	BPMG	250	1	172	2	32	107	2
HD 182681	-	15	4			-	-	
HD 191089	-	139	7	180	2	55	80	2
HD 192758	IC2391	56	4			-	-	
HD 196544	-	1.8	5			-	-	
GJ 803	BPMG	23	1	290	2	90	127	2
HD 206893	-	23	4			-	-	
Fomalhaut	-	8	7	259	2	66	156	2

Note. — The columns in order from left to right are: (1) target name, (2) membership in association, (3) fractional disk luminosity and (4) associated reference, (5) disk size in AU and (6) associated reference, (7) disk inclination to the line of sight and (8) associated reference. References: (1) Rebull et al. (2008) (2) Catalog of Resolved Debris Disks (<http://circumstellardisks.org/>). (3) Zuckerman et al. (2011) (4) Moór et al. (2006) (5) Morales et al. (2011) (6) Su et al. (2006) (7) Rhee et al. (2007) (8) Hillenbrand et al. (2008) (9) Low et al. (2005) (10) Chen et al. (2006) (1i) Wahhaj et al. (2007) (1b) Henry et al. (1996) (2b) Gray et al. (2003) (3b) Wright et al. (2004) (4b) Gray et al. (2006) (5b) Jenkins et al. (2006) (6b) Jenkins et al. (2008) (7b) Martínez-Arnáiz et al. (2010).

Table 4. 95% completeness CH_4 and H -band contrasts (Δmag)

Target	0.36''	0.5''	0.75''	1''	1.5''	2''	3''	4''	5''	7''	Cov.	9''	Cov.	12''	Cov.	14.8''	Cov.
HR 9, CH_4	11.0	12.6	13.6	14.1	14.8	15.0	15.1	15.0	15.1	14.8	0.98	14.5	0.74	13.7	0.35	12.9	0.07
HR 9, H -band	-	-	-	1.4	14.1	15.3	16.5	16.6	17.0	17.0	0.85	17.0	0.58	16.9	0.24	16.5	0.03
HIP 1481, CH_4	10.7	11.9	13.2	13.6	14.0	14.2	14.1	14.1	14.0	13.9	0.99	13.4	0.74	12.4	0.31	-	-
HIP 1481, H -band	-	-	11.5	12.8	14.4	15.2	15.5	15.6	15.4	15.4	0.89	15.0	0.65	13.6	0.31	13.6	0.06
49 Cet, CH_4	10.7	12.4	13.4	14.0	14.6	14.9	14.9	14.8	14.6	14.2	1.00	13.3	0.84	12.4	0.47	12.1	0.10
49 Cet, H -band	-	-	4.0	13.2	14.8	15.9	16.8	16.9	16.8	16.6	0.89	16.3	0.66	15.8	0.32	15.3	0.07
HD 10939, CH_4	7.6	9.6	11.8	13.1	14.2	14.5	14.6	14.6	14.5	14.5	0.93	14.4	0.68	14.0	0.30	13.5	0.06
HIP 10679, CH_4	11.0	12.3	13.3	13.9	14.4	14.6	14.7	14.8	14.6	14.5	0.93	14.2	0.68	13.7	0.28	13.0	0.05
HD 15115, CH_4	11.4	13.0	14.1	14.5	15.0	15.1	15.2	15.0	15.0	14.9	0.98	14.6	0.71	13.8	0.29	13.1	0.04
HD 15115, H -band	9.4	11.2	12.8	14.1	15.8	16.4	16.8	16.8	16.9	16.8	0.86	16.6	0.60	16.1	0.26	15.4	0.06
HD 17848, CH_4	10.5	11.8	13.0	13.8	14.5	14.8	14.9	14.9	14.8	14.7	0.99	14.4	0.76	13.8	0.32	13.3	0.06
HD 17848, H -band	-	-	-	-	14.4	15.6	16.9	17.1	17.2	17.0	0.87	16.8	0.63	16.4	0.28	15.8	0.05
HD 19668, H -band	8.1	9.9	11.5	12.8	14.4	15.1	15.1	15.1	15.1	14.9	0.89	14.7	0.63	14.0	0.27	13.2	0.04
HD 21997, CH_4	11.5	12.7	13.4	14.1	14.3	14.3	14.2	14.1	14.0	13.6	1.00	12.4	1.00	12.0	0.57	12.5	0.12
HD 21997, H -band	-	-	10.6	12.5	14.3	15.4	16.1	16.2	16.1	16.5	0.84	16.6	0.57	16.5	0.23	16.4	0.02
ϵ Eri, CH_4	-	12.7	15.0	16.0	17.2	17.5	17.7	17.6	17.5	16.9	0.46	19.8	0.46	18.6	0.46	18.2	0.46
ϵ Eri, H -band	-	-	-	-	15.8	17.0	18.5	19.0	19.9	20.3	0.90	20.2	0.67	19.3	0.33	18.6	0.07
HD 24966, CH_4	11.4	12.8	13.5	13.9	14.3	14.3	14.3	14.1	13.9	13.7	1.00	12.3	0.99	11.7	0.62	11.9	0.19
HD 24966, H -band	-	6.3	12.4	13.3	14.9	15.3	15.8	15.7	15.5	15.3	0.89	14.9	0.67	14.3	0.32	13.9	0.06
HD 25457, CH_4	11.7	13.1	14.3	15.1	15.4	15.6	15.7	15.3	15.5	15.4	0.99	14.9	0.78	14.1	0.35	14.0	0.07
HD 25457, H -band	9.2	10.8	11.6	12.0	13.6	14.6	16.1	16.7	17.1	17.1	0.87	16.9	0.62	16.4	0.27	15.7	0.04
HD 27290, CH_4	11.8	13.2	14.5	15.2	15.2	15.6	15.4	15.3	15.3	15.0	1.00	14.6	0.83	14.0	0.44	13.0	0.05
HD 27290, H -band	-	6.4	12.0	12.6	14.9	16.2	17.7	17.9	18.3	18.4	0.88	18.5	0.64	17.7	0.32	16.6	0.06
HD 31295, CH_4	11.1	12.8	13.8	14.7	15.1	15.3	15.4	15.2	15.3	15.0	0.98	14.7	0.72	13.6	0.28	13.1	0.02
HD 31295, H -band	-	-	-	-	14.9	16.0	17.0	17.2	17.3	17.2	0.86	17.1	0.62	16.5	0.27	14.4	0.04
HD 32297, CH_4	11.2	12.5	13.1	13.6	13.9	13.9	13.9	13.9	13.9	13.7	0.97	13.3	0.70	12.1	0.27	11.9	0.04
HD 32297, H -band	-	-	11.5	12.7	14.6	15.1	15.3	15.2	15.2	15.1	0.85	15.0	0.60	14.8	0.25	14.3	0.03
HIP 25486, CH_4	11.9	13.2	14.3	14.9	15.3	15.6	15.7	15.4	15.2	15.1	0.99	14.6	0.82	13.7	0.42	13.1	0.04
HIP 25486, H -band	-	-	-	13.1	14.4	15.7	16.5	16.6	16.7	16.6	0.88	16.4	0.65	15.7	0.29	14.8	0.05
HD 37484, CH_4	11.4	12.7	13.6	14.1	14.5	14.8	15.1	14.9	15.1	15.0	1.00	14.4	1.00	13.7	0.78	13.5	0.17
HD 38207, CH_4	10.6	11.8	12.5	13.0	13.5	13.6	13.5	13.6	13.5	13.2	0.98	12.8	0.73	11.5	0.28	11.6	0.05
HD 38206, CH_4	11.5	12.8	13.7	14.3	14.8	14.8	14.8	14.7	14.6	14.4	1.00	13.7	0.86	13.0	0.47	12.5	0.06
HD 38206, H -band	-	-	-	12.6	14.6	15.4	16.1	16.2	16.2	16.2	0.86	16.1	0.60	15.8	0.25	14.9	0.03
ζ Lep, CH_4	11.1	12.5	13.7	14.6	15.5	15.6	15.6	15.4	15.4	15.3	0.99	14.9	0.81	14.3	0.43	13.3	0.07
ζ Lep, H -band	-	-	-	-	-	15.1	16.6	17.2	17.6	17.5	0.92	17.6	0.74	16.9	0.37	15.7	0.09

Table 4—Continued

Target	0.36''	0.5''	0.75''	1''	1.5''	2''	3''	4''	5''	7''	Cov.	9''	Cov.	12''	Cov.	14.8''	Cov.
β Pic, CH_4	10.8	12.2	13.4	14.3	14.9	15.0	15.0	15.0	15.0	15.0	1.00	14.6	0.96	13.9	0.60	12.8	0.17
β Pic, H -band	-	-	-	-	15.1	16.4	18.0	18.6	18.9	18.7	1.00	18.5	0.94	18.3	0.53	18.0	0.22
HD 40136, CH_4	11.5	12.8	14.3	15.0	15.6	15.7	15.8	15.6	15.6	15.4	0.99	15.1	0.77	14.5	0.34	13.8	0.07
HD 40136, H -band	-	-	-	-	14.9	15.9	17.5	18.0	18.3	18.5	0.87	18.6	0.61	18.2	0.24	17.8	0.03
HD 53143, CH_4	11.1	12.6	13.8	14.6	15.0	15.4	15.2	15.2	15.2	15.1	1.00	14.9	0.79	14.2	0.29	13.5	0.04
HD 53143, H -band	-	-	-	1.3	13.5	14.6	15.8	16.1	16.2	16.2	0.86	16.1	0.61	15.8	0.28	15.0	0.04
HD 54341, CH_4	10.9	12.2	13.2	13.8	14.2	14.4	14.4	14.1	14.1	13.7	1.00	12.5	0.89	11.8	0.52	12.0	0.07
HD 54341, H -band	-	-	3.5	12.4	13.9	14.9	15.6	15.7	15.5	15.3	0.89	15.0	0.67	14.6	0.32	14.2	0.06
HD 61005, CH_4	11.0	12.4	13.4	14.0	14.4	14.1	14.1	14.1	14.0	13.5	1.00	12.9	1.00	11.6	0.82	11.0	0.15
HD 61005, H -band	-	4.6	10.1	11.9	14.2	14.9	15.0	14.9	15.0	15.0	0.86	14.9	0.60	14.7	0.24	14.4	0.03
HD 71155, CH_4	11.8	13.3	14.6	15.4	15.8	15.8	15.7	15.8	15.8	15.7	0.98	15.2	0.74	14.4	0.31	13.9	0.04
HD 71155, H -band	-	-	-	-	-	16.9	18.0	18.3	18.4	18.7	0.99	18.7	0.76	18.4	0.14	16.8	0.06
HD 85672, CH_4	11.3	12.8	13.5	14.0	14.5	14.4	14.4	14.3	14.3	14.3	0.99	13.9	0.73	12.1	0.25	12.5	0.03
HD 85672, H -band	7.6	9.4	11.6	12.9	14.5	14.7	14.7	14.9	14.9	14.8	0.86	14.6	0.61	14.1	0.26	12.6	0.03
TWA 7, CH_4	11.1	12.2	13.2	13.6	14.1	14.3	14.3	14.4	14.4	14.3	1.00	13.8	1.00	12.9	0.73	12.6	0.27
TWA 7, H -band	7.8	9.1	10.6	12.3	14.3	15.2	15.3	15.7	15.5	15.4	0.90	15.0	0.67	13.6	0.29	13.7	0.05
TW Hya, CH_4	10.5	11.6	12.5	12.8	13.4	13.5	13.7	13.7	13.7	13.2	1.00	11.8	1.00	10.6	0.69	11.9	0.20
TW Hya, H -band	7.4	9.3	11.7	13.0	14.4	14.9	14.9	15.0	14.9	15.1	0.88	14.7	0.63	14.0	0.26	13.4	0.04
TWA 13A, CH_4	10.7	12.1	12.7	13.0	13.4	13.4	13.3	13.4	13.1	13.1	0.95	13.1	0.65	12.7	0.32	12.1	0.07
TWA 13A, H -band	5.9	7.8	10.1	11.6	13.5	13.9	14.0	13.9	13.9	13.9	0.86	13.9	0.61	13.5	0.23	13.0	0.02
TWA 13B, CH_4	10.0	11.2	12.2	12.6	12.8	12.9	12.9	12.8	12.7	12.7	1.00	12.2	0.85	11.2	0.33	11.0	0.04
HD 102647, CH_4	-	-	13.4	14.5	15.3	15.9	16.0	16.0	16.0	15.9	0.98	15.8	0.70	15.4	0.26	14.2	0.02
HD 102647, H -band	-	-	-	-	14.5	15.2	16.5	17.5	17.9	18.3	0.86	18.5	0.61	18.4	0.26	17.2	0.04
HD 107146, CH_4	11.0	12.2	13.4	14.3	14.9	15.1	15.1	15.1	15.1	14.9	0.98	14.2	0.76	12.9	0.33	12.8	0.03
HD 107146, H -band	-	-	4.2	13.6	15.0	15.9	16.5	16.7	16.8	16.7	0.85	16.5	0.60	16.3	0.26	15.6	0.03
HD 109085, CH_4	-	7.4	14.3	15.2	15.8	16.0	16.0	15.8	15.6	15.6	1.00	15.1	0.95	14.2	0.48	12.1	0.01
HD 109085, H -band	12.1	12.8	12.7	12.9	14.0	15.3	16.6	17.1	17.5	17.7	0.91	17.6	0.70	17.2	0.32	16.7	0.07
HR 4796A, CH_4	11.6	12.6	13.6	14.0	14.8	15.0	15.0	15.1	14.8	14.8	0.99	14.7	0.78	14.0	0.34	13.6	0.07
HR 4796A, H -band	-	-	12.3	13.4	15.2	15.9	16.2	16.2	16.1	15.8	0.90	15.4	0.70	14.6	0.34	15.8	0.01
HD 110058, CH_4	11.1	12.2	12.9	13.3	13.7	13.8	13.8	13.6	13.7	13.3	0.99	12.8	0.78	11.8	0.35	11.7	0.07
HD 110058, H -band	9.0	10.0	11.4	12.7	14.0	14.6	14.5	14.4	14.4	14.2	0.88	13.9	0.66	13.5	0.31	13.1	0.06
HD 110411, CH_4	12.1	13.4	14.4	14.9	15.7	15.6	15.8	15.6	15.4	15.4	0.98	15.2	0.74	14.6	0.28	13.8	0.05
HD 110411, H -band	-	-	-	14.0	15.7	16.6	17.4	17.7	17.6	17.5	0.87	17.4	0.63	17.1	0.26	16.7	0.04
HD 131835, CH_4	11.1	12.4	13.1	13.3	13.7	13.8	13.7	13.7	13.6	13.3	1.00	12.3	0.84	11.3	0.43	11.5	0.10
HD 131835, H -band	8.5	9.8	12.0	13.1	14.4	14.9	15.0	14.9	15.0	14.8	1.00	14.2	1.00	13.6	0.74	13.4	0.14

Table 4—Continued

Target	0.36''	0.5''	0.75''	1''	1.5''	2''	3''	4''	5''	7''	Cov.	9''	Cov.	12''	Cov.	14.8''	Cov.
HD 138965, CH_4	10.9	12.2	13.4	13.9	14.5	14.8	14.9	14.9	15.0	14.9	1.00	13.9	0.84	12.8	0.38	13.8	0.03
HD 139664, CH_4	11.6	12.9	14.5	15.2	15.8	15.7	15.7	15.8	15.6	15.6	1.00	15.3	0.78	14.7	0.33	14.2	0.03
HD 139664, H -band	-	-	-	-	13.8	14.9	16.4	17.2	17.4	17.2	0.91	16.8	0.67	15.4	0.30	15.4	0.05
HD 141569, CH_4	12.5	14.0	14.7	15.2	15.5	15.6	15.5	15.3	15.4	15.1	1.00	15.0	0.90	14.5	0.57	13.9	0.18
HD 141569, H -band	-	10.1	11.7	13.0	14.7	15.5	15.6	15.6	15.6	15.3	0.88	14.9	0.65	14.4	0.27	14.1	0.04
HD 157728, CH_4	12.1	13.5	14.7	15.0	15.4	15.6	15.5	15.4	15.5	15.3	0.93	15.1	0.68	14.5	0.28	13.9	0.05
HD 157728, H -band	-	-	-	14.0	15.7	16.4	16.7	16.9	17.1	16.9	0.84	16.7	0.59	16.5	0.28	15.5	0.04
HIP 85340, CH_4	11.9	13.3	14.7	15.6	16.1	16.3	16.2	16.1	16.2	16.2	0.98	16.1	0.73	15.5	0.28	14.9	0.05
γ Oph, CH_4	11.3	13.0	14.3	14.8	15.3	15.5	15.5	15.5	15.4	15.3	1.00	15.1	0.79	14.5	0.29	13.9	0.04
γ Oph, H -band	9.2	10.8	12.0	12.8	15.0	15.9	17.2	17.5	17.6	17.7	0.88	17.8	0.62	17.6	0.25	17.1	0.03
HD 170773, CH_4	9.8	11.8	13.6	14.4	15.3	15.2	15.5	15.5	15.4	15.2	0.91	14.8	0.68	14.0	0.31	13.6	0.06
HD 170773, H -band	-	-	3.7	12.7	14.9	16.1	17.0	17.0	17.0	17.1	1.00	17.0	0.75	16.1	0.13	15.3	0.01
HD 172555, CH_4	11.1	12.9	14.2	14.9	15.3	15.3	15.4	15.3	15.4	15.2	1.00	14.8	0.85	14.4	0.34	12.5	0.03
HD 172555, H -band	-	-	-	1.4	14.2	15.6	16.9	17.3	17.5	17.6	0.87	17.6	0.63	17.3	0.25	16.9	0.03
HD 176638, CH_4	10.9	12.4	13.7	14.6	15.2	15.1	15.1	15.1	14.8	14.8	0.95	14.4	0.76	13.8	0.38	13.3	0.10
HD 176638, H -band	-	-	-	13.1	15.0	16.3	17.1	17.4	17.5	17.5	0.85	17.4	0.60	17.3	0.25	17.2	0.03
HR 7329, CH_4	10.6	11.8	12.9	13.6	14.4	14.6	14.8	14.6	14.7	14.5	0.98	14.3	0.76	13.7	0.32	13.1	0.06
HR 7329, H -band	-	-	-	1.4	14.4	15.5	16.6	16.7	16.8	16.9	0.88	16.7	0.63	16.0	0.26	15.7	0.04
HIP 95270, CH_4	12.1	13.3	14.1	14.6	14.9	14.9	15.1	15.0	14.9	14.7	0.99	14.2	0.80	12.6	0.37	12.5	0.07
HIP 95270, H -band	-	-	12.6	14.0	15.7	16.3	16.7	16.7	16.9	16.6	0.87	16.4	0.63	16.1	0.26	15.6	0.04
HD 182681, H -band	-	-	11.0	12.8	14.7	15.8	16.4	16.4	16.4	16.4	0.88	16.3	0.60	16.0	0.23	15.6	0.02
HD 191089, CH_4	10.6	12.1	13.4	14.0	14.5	14.7	14.7	14.7	14.8	14.5	0.95	14.3	0.75	13.9	0.33	13.0	0.07
HD 191089, H -band	-	-	11.6	12.6	14.1	14.9	15.2	15.1	15.1	14.5	1.00	13.8	0.95	13.2	0.51	13.1	0.18
HD 192758, CH_4	11.0	12.5	13.6	14.1	14.5	14.5	14.6	14.6	14.5	14.3	0.93	14.0	0.73	13.5	0.35	12.9	0.09
HD 196544, CH_4	10.1	12.2	13.5	14.6	15.2	15.5	15.5	15.5	15.6	15.6	0.98	15.4	0.72	14.8	0.27	14.6	0.04
HD 196544, H -band	-	-	4.2	14.0	15.4	16.3	17.3	17.5	17.4	17.4	0.87	17.1	0.63	16.5	0.28	15.8	0.05
GJ 803, CH_4	11.0	12.4	13.7	14.5	14.8	15.1	15.0	14.9	14.8	14.5	1.00	13.9	0.94	13.2	0.50	12.3	0.11
GJ 803, H -band	9.1	10.2	11.8	13.1	14.6	15.3	15.4	15.4	15.4	15.2	0.95	14.8	0.78	14.2	0.41	13.6	0.12
HD 206893, H -band	-	-	13.2	14.4	16.0	16.6	16.8	16.8	16.8	16.4	0.92	15.9	0.74	15.2	0.39	15.0	0.11
Fomalhaut, CH_4	-	6.5	12.9	13.9	15.4	16.1	16.7	16.6	16.7	16.4	1.00	16.1	1.00	15.3	0.50	14.4	0.08
Fomalhaut, H -band	-	-	-	-	-	-	18.9	19.8	20.6	21.3	0.87	21.7	0.61	21.5	0.27	20.1	0.04

Note. — Contrasts achieved in the CH_4 and H -bands. Beyond 6.3'' only a fraction of each final image has data, so the coverage fraction is given in the column next to the contrast. All the contrasts are 95% completeness contrasts, except at separations beyond 6.3'' where the nominal 1σ contrast curve is used.

A constant is added to the 1σ curve so that both curves match at $6.3''$.

Table 5. Lowest-Mass Companion Detectable at Different Projected Separations (M_{Jup}).

Target	0.36''	0.5''	0.75''	1''	2''	4''	8''	at disk edge
HR 9	7.4	5.7	5.0	4.6	3.6	2.4	2.2	2.7
HIP 1481	10.0	8.4	7.6	6.8	5.0	4.3	4.3	-
49 Cet	14.8	10.3	9.6	9.2	6.7	5.5	5.5	6.2
HD 10472	-	-	8.9	7.9	5.4	5.0	5.0	4.9
HD 10939	-	60.7	35.9	27.8	24.7	24.7	24.6	-
HIP 10679	6.0	5.0	4.0	3.6	3.2	3.0	3.0	-
HD 15115	6.7	5.3	4.3	4.0	2.5	2.2	2.2	2.2*
HD 17848	42.6	35.8	29.3	26.5	19.3	16.1	16.1	-
HD 19668	25.1	18.0	14.2	12.9	7.9	7.8	7.8	-
HD 21997	29.3	21.2	21.2	20.5	15.4	10.6	10.6	-
ϵ Eri	-	31.3	24.3	19.8	15.2	10.9	8.5	8.5*
HD 24966	17.9	15.1	14.3	13.9	10.8	9.0	9.0	-
HD 25457	15.1	13.9	10.8	9.8	9.5	6.0	5.3	-
HD 27290	31.8	25.0	21.1	17.5	17.1	9.7	9.7	-
HD 31295	28.9	22.7	21.3	19.6	14.8	12.2	12.2	-
HD 32297	28.3	22.1	20.6	20.5	15.5	15.5	15.5	14.7
HIP 25486	5.8	4.9	3.9	3.5	2.8	2.0	2.0	2.0
HD 37484	10.6	8.4	8.0	7.4	6.2	6.0	6.0	-
HD 38207	9.1	7.9	7.1	6.8	6.5	6.4	6.4	-
HD 38206	10.3	9.3	8.2	8.1	6.3	5.6	5.6	-
ζ Lep	19.4	12.4	12.4	12.4	10.8	8.0	7.0	-
β Pic	7.8	6.4	5.3	4.6	2.9	1.3	1.3	1.3*
HD 40136	32.1	25.5	21.0	17.5	11.1	11.1	10.7	-
HD 53143	25.6	21.2	17.6	14.7	13.2	9.5	9.5	10.3
HD 54341	25.1	20.0	18.4	17.3	15.7	13.1	13.1	-
HD 61005	14.7	13.8	10.8	9.6	8.1	7.9	7.9	7.7
HD 71155	30.4	25.6	22.4	19.6	16.9	10.7	9.3	-
HD 85672	27.1	20.7	19.6	18.7	14.9	14.8	14.8	-
TWA 7	3.9	3.3	2.5	2.1	1.2	1.0	1.0	-
TW Hya	5.9	4.9	4.3	3.8	2.5	2.4	2.4	2.4
TWA 13A	5.5	4.4	3.9	3.7	3.1	3.1	3.1	-
TWA 13B	5.7	4.7	3.8	3.6	3.4	3.4	3.4	-
HD 102647	-	-	21.2	19.5	15.2	10.4	7.4	12.8
HD 107146	16.3	18.6	15.9	12.2	9.5	7.2	7.2	7.2
HD 109085	12.2	14.4	13.5	10.8	9.7	7.1	5.7	6.3
HR 4796 A	7.1	5.9	5.0	4.7	3.4	3.2	3.2	4.6
HD 110058	13.8	10.8	10.2	10.1	7.9	7.9	7.9	-
HD 110411	12.9	13.5	13.1	11.2	8.4	5.7	5.7	-
HD 131835	35.8	29.0	26.4	25.5	19.2	19.2	19.2	-
HD 138965	23.5	20.4	17.7	17.2	14.8	14.5	14.5	-
HD 139664	23.3	19.2	14.8	10.7	10.6	8.4	8.4	8.2
HD 141569	4.1	3.2	2.8	2.5	2.4	2.3	2.3	2.3
HD 157728	12.4	14.0	12.1	10.8	9.1	7.5	7.5	-
HIP 85340	50.7	41.4	31.4	28.5	27.7	27.1	26.3	-
γ Oph	35.8	26.3	24.6	24.5	18.5	15.2	13.8	13.8*
HD 170773	30.6	21.4	19.4	15.4	13.4	9.0	8.9	-

Table 5—Continued

Target	0.36''	0.5''	0.75''	1''	2''	4''	8''	at disk edge
HD 172555	7.8	5.9	4.9	4.2	3.7	2.3	2.0	2.4
HD 176638	35.2	29.7	23.3	21.5	16.2	13.7	13.4	-
HR 7329	8.6	7.2	6.0	5.4	3.9	3.0	2.9	3.8
HIP 95270	6.1	5.2	4.4	4.0	2.6	2.3	2.3	3.4
HD 182681	-	-	24.5	21.7	12.7	9.9	9.9	-
HD 191089	7.7	6.1	5.1	4.4	3.8	3.6	3.6	3.9
HD 192758	11.0	9.9	9.2	8.9	7.7	7.6	7.6	-
HD 196544	40.3	26.8	23.6	20.8	16.8	11.9	11.9	-
GJ 803	5.1	3.8	2.8	2.2	1.6	1.6	1.6	1.6*
HD 206893	-	-	19.4	14.6	9.4	8.9	8.9	-
Fomalhaut	-	-	35.2	31.0	22.4	12.0	8.6	8.6*

Note. — The last column gives the lowest mass companion detectable at the outer radius of the debris disk, using the radius estimate from Table 3. If the disk radius is too large (falls outside of the NICI field of view), we present the mass limit at the edge of the field (marked with * in table). If the disk radius falls inside the coronagraph, we do not present the mass limit.

Table 6. Properties of Candidate Companions

Name	#	Sep (")	PA (deg)	ΔH (mag)	$\Delta\tau$ (years)	Epochs	χ^2_{ν} (BG)	χ^2_{ν} (CPM)	dof	Comp?
HD 19668	1	5.476	150.7	10.1	9.93	8	0.73	34.93	14	BG
HD 27290	1	7.745	244.0	10.6	1.05	2	1.64	106.91	2	BG
HD 31295	1	6.261	271.6	13.3	1.95	2	0.09	69.71	2	BG
HD 31295	2	8.805	316.7	14.5	1.95	2	0.02	187.48	2	BG
ζ Lep	1	5.295	110.0	18.0	2.24	2	0.55	28.93	2	BG
HD 53143	1	4.479	286.2	10.3	0.98	2	2.62	163.81	2	BG
HD 54341	1	3.080	131.2	12.7	2.03	2	0.36	3.05	2	BG
HD 54341	2	4.372	137.3	11.8	2.03	2	0.98	2.56	2	BG
HD 61005	1	3.601	326.4	13.4	2.28	2	0.43	210.25	2	BG
HD 61005	2	6.388	315.3	12.6	2.28	2	0.78	190.35	2	BG
HD 61005	3	7.185	191.5	13.6	2.28	2	2.93	62.73	2	BG
HD 71155	1	5.766	86.7	-99.0	2.41	3	0.84	65.12	4	BG
HD 71155	2	7.360	357.8	-99.0	2.41	2	0.02	19.78	2	BG
HD 71155	3	9.403	246.1	-99.0	2.41	2	1.15	95.44	2	BG
TWA 7	1	3.200	121.5	8.6	1.05	2	0.43	64.79	2	BG
TWA 7	2	3.937	92.6	14.5	1.05	2	0.09	58.64	2	BG
TWA 7	3	4.939	173.1	13.6	1.05	2	1.62	30.05	2	BG
HD 107146	1	6.723	217.6	14.4	1.23	2	2.35	184.97	2	BG
HD 138965	1	1.708	61.4	10.6	2.20	2	0.84	75.76	2	BG
HD 138965	2	4.085	244.6	12.2	2.20	2	0.19	81.31	2	BG
HD 138965	3	4.284	269.6	14.6	2.20	2	0.51	35.10	2	BG
HD 138965	4	7.386	157.3	11.4	2.20	2	0.46	35.91	2	BG
HD 138965	5	7.503	102.1	12.8	2.20	2	0.98	36.51	2	BG
HD 138965	6	7.838	236.4	11.4	2.20	2	0.01	75.49	2	BG
HD 138965	7	8.048	326.9	11.3	2.20	2	0.17	17.66	2	BG
HD 138965	8	9.970	4.4	13.6	2.20	2	1.22	41.08	2	BG
HD 139664	1	1.945	47.6	15.8	1.25	2	1.20	529.62	2	BG
HD 139664	2	5.620	94.4	16.3	1.25	2	0.35	232.61	2	BG
HD 139664	3	6.218	115.3	15.0	1.25	2	0.04	125.15	2	BG
HD 139664	4	6.777	2.4	15.1	1.25	2	0.04	429.75	2	BG
γ Oph	1	4.500	59.5	14.6	1.07	2	1.70	30.67	2	BG
γ Oph	2	5.886	239.4	16.0	1.07	2	0.32	9.62	2	BG
γ Oph	3	6.203	267.3	12.6	1.07	2	0.26	5.48	2	BG
γ Oph	4	6.581	275.0	15.0	1.07	2	1.44	4.42	2	BG
γ Oph	5	6.962	59.8	13.6	1.07	2	1.43	21.95	2	BG
γ Oph	6	8.689	96.2	12.3	1.07	2	1.11	8.06	2	BG
γ Oph	7	9.240	253.4	15.5	1.07	2	2.59	3.15	2	BG
HD 170773	1	4.591	232.4	16.0	0.47	2	0.17	11.52	2	BG
HD 170773	2	4.751	219.9	14.7	0.47	2	0.15	9.02	2	BG
HD 170773	3	4.793	96.4	15.8	0.47	2	0.16	24.09	2	BG
HD 170773	4	6.899	113.6	15.1	0.47	2	0.13	26.14	2	BG
HD 170773	5	7.575	51.9	14.0	1.63	4	0.76	4.82	6	BG
HD 170773	6	7.684	44.6	15.3	0.47	2	0.02	7.61	2	BG
HD 170773	7	7.802	327.9	15.6	0.47	2	1.19	13.14	2	BG
HD 170773	8	7.866	343.8	14.2	0.47	2	1.36	7.00	2	BG

Table 6—Continued

Name	#	Sep (")	PA (deg)	ΔH (mag)	$\Delta\tau$ (years)	Epochs	χ^2_{ν} (BG)	χ^2_{ν} (CPM)	dof	Comp?
HD 170773	9	7.879	161.1	14.3	0.47	2	0.08	13.34	2	BG
HD 170773	10	7.921	337.3	13.3	1.63	3	2.83	19.88	4	BG
HD 170773	11	7.964	141.5	14.7	0.47	2	0.05	25.39	2	BG
HD 170773	12	8.262	263.9	13.5	1.63	4	2.96	13.21	6	BG
HD 170773	13	8.490	213.2	11.3	1.63	4	3.17	13.02	6	BG
HD 170773	14	9.150	313.7	15.8	0.47	2	0.83	18.86	2	BG
HD 170773	15	9.696	245.3	15.6	0.47	2	0.09	14.70	2	BG
HD 170773	16	10.030	265.4	13.7	1.63	4	3.04	14.22	6	BG
HD 170773	17	10.424	136.7	13.5	1.63	3	3.83	100.53	4	BG
HD 170773	18	11.722	184.5	14.8	0.43	2	0.10	2.92	2	BG
HD 170773	19	12.435	313.0	-99.0	1.63	2	6.56	54.05	2	BG
HD172555	1	7.730	318.9	14.5	3.92	2	0.01	12.11	2	BG
HD 176638	1	3.500	157.8	14.1	0.47	2	0.36	8.35	2	BG
HD 176638	2	4.723	93.4	12.6	0.90	3	0.42	6.25	4	BG
HD 176638	3	5.233	265.6	14.5	0.47	2	0.04	11.25	2	BG
HD 176638	4	9.416	319.6	10.6	0.90	3	3.60	5.43	4	BG
HIP95270	1	4.920	254.6	13.1	3.95	2	0.08	5.08	2	BG
HIP95270	2	6.040	276.6	11.8	3.95	2	0.04	4.36	2	BG
HD 196544	1	4.352	93.4	14.5	2.63	5	3.51	10.24	8	BG
HD 196544	2	4.743	90.8	13.1	2.63	5	0.42	12.49	8	BG
HD 206893	1	6.211	158.3	15.7	0.90	2	0.37	7.56	2	BG

Note. — Summary of the candidate companions detected around each target star. For each candidate we list the separation and position angle at the reference epoch, the contrast between candidate and host star, the time baseline for our astrometric data, the number of epochs, the reduced chi-square statistic for the companion to be background (BG) or common proper motion (CPM), the number of degrees of freedom, and the final determination of each companion: background or common proper motion. Astrometry for individual epochs is in Table 7.

Table 7. Astrometry of Candidate Companions

Name	#	Epoch	Measured Position				Background Position				Inst.	Comp?
			Sep (")	σ_{Sep}	PA (deg)	σ_{PA}	Sep (")	σ_{Sep}	PA (deg)	σ_{PA}		
HD 19668	1	2010.66	5.476	0.009	150.7	0.2	N	BG
		2001.93	6.781	0.144	149.1	1.3	6.726	0.015	148.583	0.185	S	BG
		2002.97	6.662	0.288	150.3	2.6	6.581	0.014	148.724	0.185	S	BG
		2009.74	5.566	0.013	150.0	0.5	5.603	0.010	150.414	0.204	V	BG
		2010.82	5.429	0.013	150.0	0.5	5.450	0.010	150.550	0.211	V	BG
		2010.98	5.408	0.009	150.7	0.2	5.437	0.010	150.356	0.213	N	BG
		2011.70	5.301	0.009	151.1	0.2	5.326	0.011	150.975	0.219	N	BG
		2011.86	5.301	0.013	151.2	0.3	5.304	0.011	150.758	0.220	L	BG
HD 27290	1	2008.96	7.745	0.009	244.0	0.2	N	BG
		2010.01	7.914	0.009	242.3	0.2	7.916	0.007	242.995	0.186	N	BG
HD 31295	1	2009.04	6.261	0.009	271.6	0.2	N	BG
		2010.98	6.368	0.009	273.9	0.2	6.362	0.009	273.794	0.196	N	BG
HD 31295	2	2009.04	8.805	0.009	316.7	0.2	N	BG
		2010.98	9.050	0.009	317.2	0.2	9.049	0.008	317.329	0.183	N	BG
ζ Lep	1	2008.95	5.295	0.009	110.0	0.2	N	BG
		2011.20	5.390	0.009	109.6	0.2	5.379	0.009	109.966	0.202	N	BG
HD 53143	1	2009.03	4.479	0.009	286.2	0.2	N	BG
		2010.01	4.302	0.009	282.9	0.2	4.268	0.009	283.413	0.220	N	BG
HD 54341	1	2008.95	3.080	0.009	131.2	0.2	N	BG
		2010.98	3.077	0.009	131.9	0.2	3.090	0.010	131.710	0.219	N	BG
HD 54341	2	2008.95	4.372	0.009	137.3	0.2	N	BG
		2010.98	4.363	0.009	137.9	0.2	4.385	0.009	137.663	0.207	N	BG
HD 61005	1	2009.03	3.601	0.009	326.4	0.2	N	BG
		2011.31	3.340	0.009	326.4	0.2	3.349	0.010	326.689	0.202	N	BG
HD 61005	2	2009.03	6.388	0.009	315.3	0.2	N	BG
		2011.31	6.142	0.009	314.6	0.2	6.138	0.010	315.052	0.180	N	BG
HD 61005	3	2009.03	7.185	0.009	191.5	0.2	N	BG
		2011.31	7.309	0.009	190.0	0.2	7.353	0.009	190.048	0.192	N	BG
HD 71155	1	2008.96	5.766	0.009	86.7	0.2	N	BG
		2009.97	5.857	0.013	85.7	0.5	5.836	0.009	86.502	0.194	V	BG
		2011.37	5.955	0.009	86.2	0.2	5.969	0.009	86.464	0.189	N	BG
HD 71155	2	2008.96	7.360	0.009	357.8	0.2	N	BG
		2011.37	7.391	0.009	359.5	0.2	7.391	0.009	359.401	0.204	N	BG
HD 71155	3	2008.96	9.403	0.009	246.1	0.2	N	BG
		2011.37	9.229	0.009	245.5	0.2	9.205	0.009	245.760	0.190	N	BG
TWA 7	1	2009.11	3.200	0.009	121.5	0.2	N	BG
		2010.16	3.316	0.009	119.5	0.2	3.304	0.011	119.795	0.183	N	BG
TWA 7	2	2009.11	3.937	0.009	92.6	0.2	N	BG
		2010.16	4.072	0.009	92.0	0.2	4.073	0.009	92.125	0.186	N	BG
TWA 7	3	2009.11	4.939	0.009	173.1	0.2	N	BG
		2010.16	4.953	0.009	170.9	0.2	4.929	0.010	171.483	0.227	N	BG
HD 107146	1	2009.03	6.723	0.009	217.6	0.2	N	BG
		2010.27	6.482	0.009	216.7	0.2	6.442	0.009	216.704	0.181	N	BG

Table 7—Continued

Name	#	Epoch	Measured Position				Background Position				Inst.	Comp?
			Sep (")	σ_{Sep}	PA (deg)	σ_{PA}	Sep (")	σ_{Sep}	PA (deg)	σ_{PA}		
HD 138965	1	2009.12	1.708	0.009	61.4	0.2	N	BG
		2011.32	1.845	0.009	59.7	0.2	1.857	0.009	59.310	0.171	N	BG
HD 138965	2	2009.12	4.085	0.009	244.6	0.2	N	BG
		2011.32	3.931	0.009	245.8	0.2	3.942	0.010	245.727	0.215	N	BG
HD 138965	3	2009.12	4.284	0.009	269.6	0.2	N	BG
		2011.32	4.200	0.009	271.1	0.2	4.188	0.009	271.417	0.203	N	BG
HD 138965	4	2009.12	7.386	0.009	157.3	0.2	N	BG
		2011.32	7.300	0.009	155.9	0.2	7.304	0.008	156.236	0.180	N	BG
HD 138965	5	2009.12	7.503	0.009	102.1	0.2	N	BG
		2011.32	7.597	0.009	100.9	0.2	7.572	0.009	100.971	0.194	N	BG
HD 138965	6	2009.12	7.838	0.009	236.4	0.2	N	BG
		2011.32	7.683	0.009	236.9	0.2	7.685	0.010	236.811	0.217	N	BG
HD 138965	7	2009.12	8.048	0.009	326.9	0.2	N	BG
		2011.32	8.112	0.009	327.8	0.2	8.106	0.009	328.008	0.184	N	BG
HD 138965	8	2009.12	9.970	0.009	4.4	0.2	N	BG
		2011.32	10.085	0.009	4.6	0.2	10.108	0.007	4.882	0.200	N	BG
HD 139664	1	2009.10	1.945	0.009	47.6	0.2	N	BG
		2010.35	2.346	0.009	45.3	0.2	2.372	0.009	45.498	0.175	N	BG
HD 139664	2	2009.10	5.620	0.009	94.4	0.2	N	BG
		2010.35	5.847	0.009	91.0	0.2	5.859	0.009	90.775	0.193	N	BG
HD 139664	3	2009.10	6.218	0.009	115.3	0.2	N	BG
		2010.35	6.318	0.009	111.4	0.2	6.313	0.009	111.427	0.188	N	BG
HD 139664	4	2009.10	6.777	0.009	2.4	0.2	N	BG
		2010.35	7.141	0.009	4.3	0.2	7.143	0.009	4.356	0.183	N	BG
γ Oph	1	2009.19	4.500	0.009	59.5	0.2	N	BG
		2010.27	4.588	0.009	58.5	0.2	4.562	0.009	58.935	0.179	N	BG
γ Oph	2	2009.19	5.886	0.009	239.4	0.2	N	BG
		2010.27	5.837	0.009	240.0	0.2	5.825	0.008	239.843	0.191	N	BG
γ Oph	3	2009.19	6.203	0.009	267.3	0.2	N	BG
		2010.27	6.183	0.009	268.2	0.2	6.172	0.010	268.010	0.213	N	BG
γ Oph	4	2009.19	6.581	0.009	275.0	0.2	N	BG
		2010.27	6.589	0.009	275.8	0.2	6.560	0.009	275.667	0.188	N	BG
γ Oph	5	2009.19	6.962	0.009	59.8	0.2	N	BG
		2010.27	7.032	0.009	58.8	0.2	7.023	0.008	59.398	0.200	N	BG
γ Oph	6	2009.19	8.689	0.009	96.2	0.2	N	BG
		2010.27	8.707	0.009	95.1	0.2	8.710	0.009	95.672	0.181	N	BG
γ Oph	7	2009.19	9.240	0.009	253.4	0.2	N	BG
		2010.27	9.229	0.009	254.1	0.2	9.192	0.008	253.783	0.212	N	BG
HD 170773	1	2011.79	4.591	0.009	232.4	0.2	N	BG
		2012.26	4.638	0.009	233.2	0.2	4.643	0.009	233.428	0.209	N	BG
HD 170773	2	2011.79	4.751	0.009	219.9	0.2	N	BG
		2012.26	4.785	0.009	220.8	0.2	4.783	0.009	221.039	0.207	N	BG
HD 170773	3	2011.79	4.793	0.009	96.4	0.2	N	BG	

Table 7—Continued

Name	#	Epoch	Measured Position				Background Position				Inst.	Comp?
			Sep (")	σ_{Sep}	PA (deg)	σ_{PA}	Sep (")	σ_{Sep}	PA (deg)	σ_{PA}		
HD 170773	4	2012.26	4.706	0.009	96.1	0.2	4.696	0.009	96.116	0.196	N	BG
		2011.79	6.899	0.009	113.6	0.2	N	BG
		2012.26	6.807	0.009	113.6	0.2	6.798	0.010	113.667	0.232	N	BG
HD 170773	5	2011.79	7.575	0.009	51.9	0.2	N	BG
		2010.63	7.586	0.013	51.5	0.5	7.598	0.010	52.829	0.209	V	BG
		2011.36	7.551	0.009	51.7	0.2	7.550	0.010	52.013	0.210	N	BG
HD 170773	6	2012.26	7.521	0.009	51.2	0.2	7.525	0.010	51.204	0.210	N	BG
		2011.79	7.684	0.009	44.6	0.2	N	BG
		2012.26	7.648	0.009	43.8	0.2	7.646	0.009	43.863	0.206	N	BG
HD 170773	7	2011.79	7.802	0.009	327.9	0.2	N	BG
		2012.26	7.860	0.009	327.2	0.2	7.884	0.008	327.438	0.196	N	BG
HD 170773	8	2011.79	7.866	0.009	343.8	0.2	N	BG
		2012.26	7.900	0.009	343.1	0.2	7.929	0.009	343.230	0.190	N	BG
HD 170773	9	2011.79	7.879	0.009	161.1	0.2	N	BG
		2012.26	7.816	0.009	161.5	0.2	7.813	0.010	161.616	0.181	N	BG
HD 170773	10	2011.79	7.921	0.009	337.3	0.2	N	BG
		2010.63	7.804	0.013	335.7	0.5	7.805	0.008	337.663	0.197	V	BG
		2012.26	7.962	0.009	336.5	0.2	7.993	0.008	336.745	0.194	N	BG
HD 170773	11	2011.79	7.964	0.009	141.5	0.2	N	BG
		2012.26	7.874	0.009	141.8	0.2	7.876	0.008	141.868	0.198	N	BG
HD 170773	12	2011.79	8.262	0.009	263.9	0.2	N	BG
		2010.63	8.247	0.013	261.4	0.5	8.176	0.009	263.216	0.206	V	BG
HD 170773	13	2011.36	8.278	0.009	263.4	0.2	8.273	0.009	263.688	0.204	N	BG
		2012.26	8.354	0.009	264.0	0.2	8.351	0.009	264.215	0.202	N	BG
		2011.79	8.490	0.009	213.2	0.2	N	BG
		2010.63	8.598	0.013	210.8	0.5	8.510	0.010	212.302	0.207	V	BG
		2011.36	8.524	0.009	212.9	0.2	8.519	0.010	213.095	0.206	N	BG
HD 170773	14	2012.26	8.504	0.009	213.7	0.2	8.510	0.010	213.828	0.207	N	BG
		2011.79	9.150	0.009	313.7	0.2	N	BG
		2012.26	9.225	0.009	313.2	0.2	9.244	0.009	313.484	0.164	N	BG
HD 170773	15	2011.79	9.696	0.009	245.3	0.2	N	BG
		2012.26	9.764	0.009	245.6	0.2	9.765	0.009	245.774	0.213	N	BG
HD 170773	16	2011.79	10.030	0.009	265.4	0.2	N	BG
		2010.63	10.012	0.013	263.1	0.5	9.942	0.009	264.844	0.189	V	BG
		2011.36	10.051	0.009	264.9	0.2	10.040	0.009	265.217	0.188	N	BG
		2012.26	10.129	0.009	265.4	0.2	10.120	0.009	265.640	0.186	N	BG
HD 170773	17	2012.26	10.424	0.009	136.7	0.2	N	BG
		2010.63	10.718	0.013	135.3	0.5	10.644	0.009	136.419	0.190	V	BG
		2011.36	10.513	0.009	136.5	0.2	10.532	0.009	136.617	0.192	N	BG
HD 170773	18	2011.79	11.722	0.009	184.5	0.2	N	BG
		2011.36	11.752	0.009	184.3	0.2	11.752	0.010	184.486	0.200	N	BG
HD 170773	19	2012.26	12.435	0.009	313.0	0.2	N	BG
		2010.63	12.276	0.013	311.6	0.5	12.212	0.009	313.182	0.240	V	BG

Table 7—Continued

Name	#	Epoch	Measured Position				Background Position				Inst.	Comp?
			Sep (")	σ_{Sep}	PA (deg)	σ_{PA}	Sep (")	σ_{Sep}	PA (deg)	σ_{PA}		
HD172555	1	2009.27	7.730	0.009	318.9	0.2	N	BG
		2005.35	7.210	0.120	316.5	1.0	7.215	0.009	316.704	0.222	H	BG
HD 176638	1	2011.79	3.500	0.009	157.8	0.2	N	BG
		2012.26	3.473	0.009	158.8	0.2	3.460	0.010	158.640	0.192	N	BG
HD 176638	2	2011.36	4.723	0.009	93.4	0.2	N	BG
		2011.79	4.732	0.009	93.3	0.2	4.728	0.009	93.145	0.193	N	BG
		2012.26	4.660	0.009	93.4	0.2	4.667	0.009	92.947	0.195	N	BG
HD 176638	3	2011.79	5.233	0.009	265.6	0.2	N	BG
		2012.26	5.293	0.009	265.7	0.2	5.291	0.010	265.831	0.189	N	BG
HD 176638	4	2011.79	9.416	0.009	319.6	0.2	N	BG
		2011.36	9.359	0.009	319.4	0.2	9.405	0.009	319.540	0.181	N	BG
		2012.26	9.420	0.009	319.4	0.2	9.470	0.009	319.443	0.180	N	BG
HIP95270	1	2009.28	4.920	0.009	254.6	0.2	N	BG
		2005.33	4.940	0.120	250.1	1.4	4.923	0.010	250.715	0.220	H	BG
HIP95270	2	2009.28	6.040	0.009	276.6	0.2	N	BG
		2005.33	5.900	0.120	273.3	1.2	5.916	0.010	273.632	0.192	H	BG
HD 196544	1	2011.31	4.352	0.009	93.4	0.2	N	BG
		2008.69	4.468	0.050	93.8	1.0	4.483	0.009	93.545	0.181	G	BG
		2009.32	4.450	0.009	94.1	1.0	4.431	0.009	93.511	0.183	N	BG
		2010.83	4.313	0.009	93.0	0.2	4.404	0.009	93.272	0.184	N	BG
		2010.91	4.404	0.020	93.6	0.5	4.399	0.009	93.222	0.184	K	BG
HD 196544	2	2011.31	4.743	0.009	90.8	0.2	N	BG
		2008.69	4.863	0.050	91.0	1.0	4.873	0.009	91.021	0.169	G	BG
		2009.32	4.836	0.009	91.3	1.0	4.821	0.009	90.962	0.171	N	BG
		2010.83	4.814	0.009	90.3	0.2	4.795	0.009	90.728	0.171	N	BG
		2010.91	4.800	0.020	90.8	0.5	4.790	0.009	90.680	0.171	K	BG
HD 206893	1	2011.83	6.211	0.009	158.3	0.2	N	BG
		2012.73	6.169	0.009	158.9	0.2	6.180	0.009	159.099	0.200	N	BG

Note. — Astrometry for each candidate companion detected around our target stars from NICI and archival observations. At each epoch we give the measured separation, position angle, and uncertainties as well as the predicted separation and position angle for a background object based on the proper motion and parallax of the primary and the candidate position at the reference epoch, which is the first epoch listed for each candidate. Astrometry is taken from NICI (N), VLT NACO (V), Keck NIRC2 (K), VLT ISAAC (I), ESO 3.6m (E), and Gemini NIRI (G).

Table 8. Single-epoch astrometry for sources with large physical separations.

Target	Obj. No.	Epoch	Sep. (AU)	Separation (")	Sep. Unc. (")	PA (deg)	PA Unc. (deg)	ΔH (mag)
HD 131835	1	2009.28	594.8	5.360	0.009	20.1	0.2	14.8
	2	2009.28	642.5	5.790	0.009	22.8	0.2	14.1
	3	2009.28	683.6	6.160	0.009	-56.0	0.2	13.6
	4	2009.28	894.5	8.060	0.009	-119.8	0.2	16.2
	5	2009.28	994.2	8.960	0.009	100.4	0.2	16.4
HD 157728	1	2011.38	491.2	11.424	0.009	-286.7	0.2	14.8
HD 172555	1	2009.27	225.7	7.730	0.009	-41.1	0.2	15.5
HD 182681	1	2010.66	313.5	4.544	0.009	-110.0	0.0	12.2
	2	2010.66	365.1	5.292	0.009	-108.7	0.0	17.2
	3	2010.66	593.1	8.595	0.009	-54.9	0.0	15.5
	4	2010.66	612.1	8.871	0.009	-70.4	0.0	14.0
	5	2010.66	659.2	9.554	0.009	-56.2	0.0	16.8

Table 9. Upper Limits on the Fraction of Stars with Planets Including β Pic b and HR 8799bcd.

	$>0.5M_{Jup}$	$>1M_{Jup}$	$>3M_{Jup}$	$>5M_{Jup}$	$>7M_{Jup}$	$>9M_{Jup}$	$>11M_{Jup}$
>0.5 AU	1.00	1.00	1.00	1.00	1.00	1.00	0.99
>5 AU	0.60	0.55	0.50	0.47	0.43	0.35	0.23
>10 AU	0.48	0.41	0.35	0.33	0.29	0.23	0.15
>20 AU	0.39	0.35	0.29	0.26	0.23	0.19	0.11
>40 AU	0.25	0.25	0.21	0.19	0.17	0.13	0.08
>80 AU	0.19	0.15	0.14	0.13	0.11	0.09	0.05
>160 AU	0.14	0.11	0.10	0.08	0.07	0.06	0.03

Note. — These are the 95% confidence-interval upper limits on the fraction of stars with ≥ 1 planet(s), when we include β Pic b and HR 8799bcd in the analysis. The limits are given for planet mass and semi-major axis greater than indicated in table and less than $13M_{Jup}$ and 1000 AU, respectively. They are calculated from the 4-dimensional probability density given as a function of the mass, SMA, SMA-cutoff and planet multiplicity. Thus unlike Figure 13, these are model-dependent constraints. Planet detections and single-epoch detections are all taken into account in these limits.

Table 10. Upper Limits on the Average Planet Multiplicity Including β Pic b and HR 8799bcd.

	$>0.5M_{Jup}$	$>1M_{Jup}$	$>3M_{Jup}$	$>5M_{Jup}$	$>7M_{Jup}$	$>9M_{Jup}$	$>11M_{Jup}$
>0.5 AU	11.33	11.10	10.95	10.54	9.62	7.72	4.68
>5 AU	0.91	0.80	0.69	0.64	0.56	0.44	0.26
>10 AU	0.65	0.53	0.44	0.39	0.34	0.27	0.16
>20 AU	0.49	0.43	0.34	0.30	0.26	0.20	0.12
>40 AU	0.29	0.28	0.24	0.22	0.18	0.14	0.08
>80 AU	0.20	0.16	0.15	0.14	0.12	0.09	0.05
>160 AU	0.15	0.12	0.10	0.09	0.08	0.06	0.03

Note. — These are the 95% confidence-interval upper limits on the average planet multiplicity, when we include β Pic b and HR 8799bcd in the analysis. Same as for Table 9, the limits are given for planet mass and semi-major axis greater than indicated in table and less than $13M_{Jup}$ and 1000 AU, respectively.

Table 11. Upper Limits on the Fraction of Stars with Planets Excluding β Pic b and HR 8799bcd.

	$>0.5M_{Jup}$	$>1M_{Jup}$	$>3M_{Jup}$	$>5M_{Jup}$	$>7M_{Jup}$	$>9M_{Jup}$	$>11M_{Jup}$
>0.5 AU	1.00	1.00	1.00	1.00	1.00	1.00	0.97
>5 AU	0.61	0.37	0.25	0.21	0.18	0.14	0.08
>10 AU	0.47	0.28	0.20	0.17	0.15	0.11	0.06
>20 AU	0.35	0.22	0.15	0.13	0.11	0.08	0.05
>40 AU	0.28	0.18	0.12	0.11	0.09	0.07	0.04
>80 AU	0.23	0.15	0.10	0.09	0.08	0.06	0.03
>160 AU	0.22	0.13	0.09	0.08	0.07	0.05	0.03

Note. — These are the 95% confidence-interval upper limits on the fraction of stars with ≥ 1 planet(s), when we exclude β Pic b and HR 8799bcd in the analysis. The limits are given for planet mass and semi-major axis greater than indicated in table and less than $13M_{Jup}$ and 1000 AU, respectively. They are calculated from the 4-dimensional probability density given as a function of the mass, SMA, SMA-cutoff and planet multiplicity. Thus unlike Figure 13, these are model-dependent constraints. Planet detections and single-epoch detections are all taken into account in these limits.

Table 12. Upper Limits on the Average Planet Multiplicity Excluding β Pic b and HR 8799bcd.

	$>0.5M_{Jup}$	$>1M_{Jup}$	$>3M_{Jup}$	$>5M_{Jup}$	$>7M_{Jup}$	$>9M_{Jup}$	$>11M_{Jup}$
>0.5 AU	10.28	8.74	8.53	8.08	7.18	5.77	3.43
>5 AU	0.94	0.46	0.29	0.24	0.20	0.15	0.08
>10 AU	0.64	0.33	0.22	0.19	0.16	0.11	0.06
>20 AU	0.44	0.25	0.17	0.14	0.12	0.09	0.05
>40 AU	0.32	0.20	0.13	0.11	0.09	0.07	0.04
>80 AU	0.26	0.17	0.11	0.09	0.08	0.06	0.03
>160 AU	0.25	0.14	0.10	0.08	0.07	0.06	0.03

Note. — These are the 95% confidence-interval upper limits on the average planet multiplicity, when we exclude β Pic b and HR 8799bcd in the analysis. Same as for Table 9, the limits are given for planet mass and semi-major axis greater than indicated in table and less than $13M_{Jup}$ and 1000 AU, respectively.

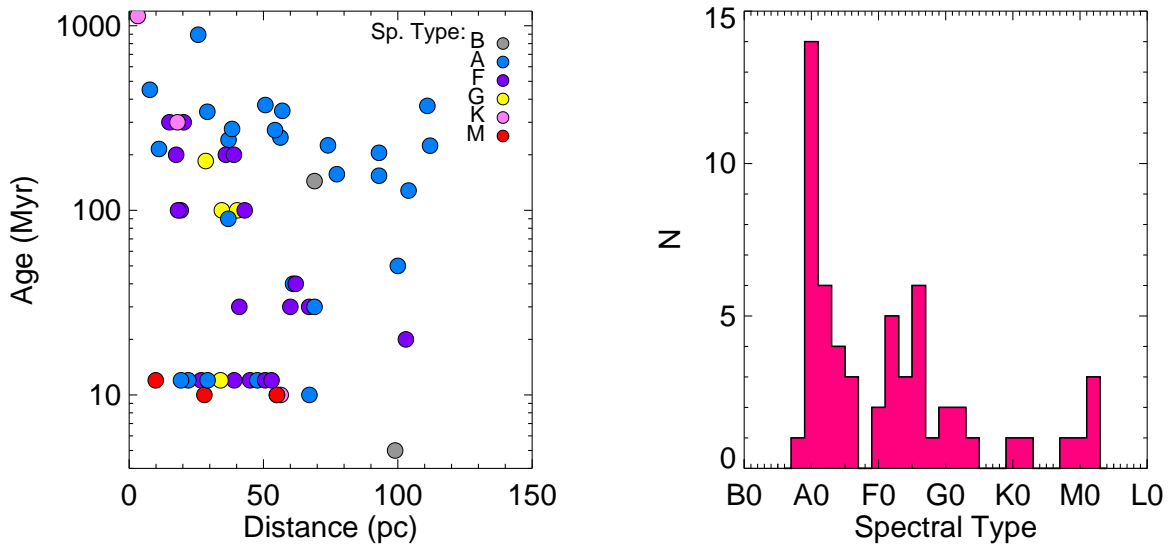


Fig. 1.— Ages, spectral types and distances of the NICI debris disk targets.

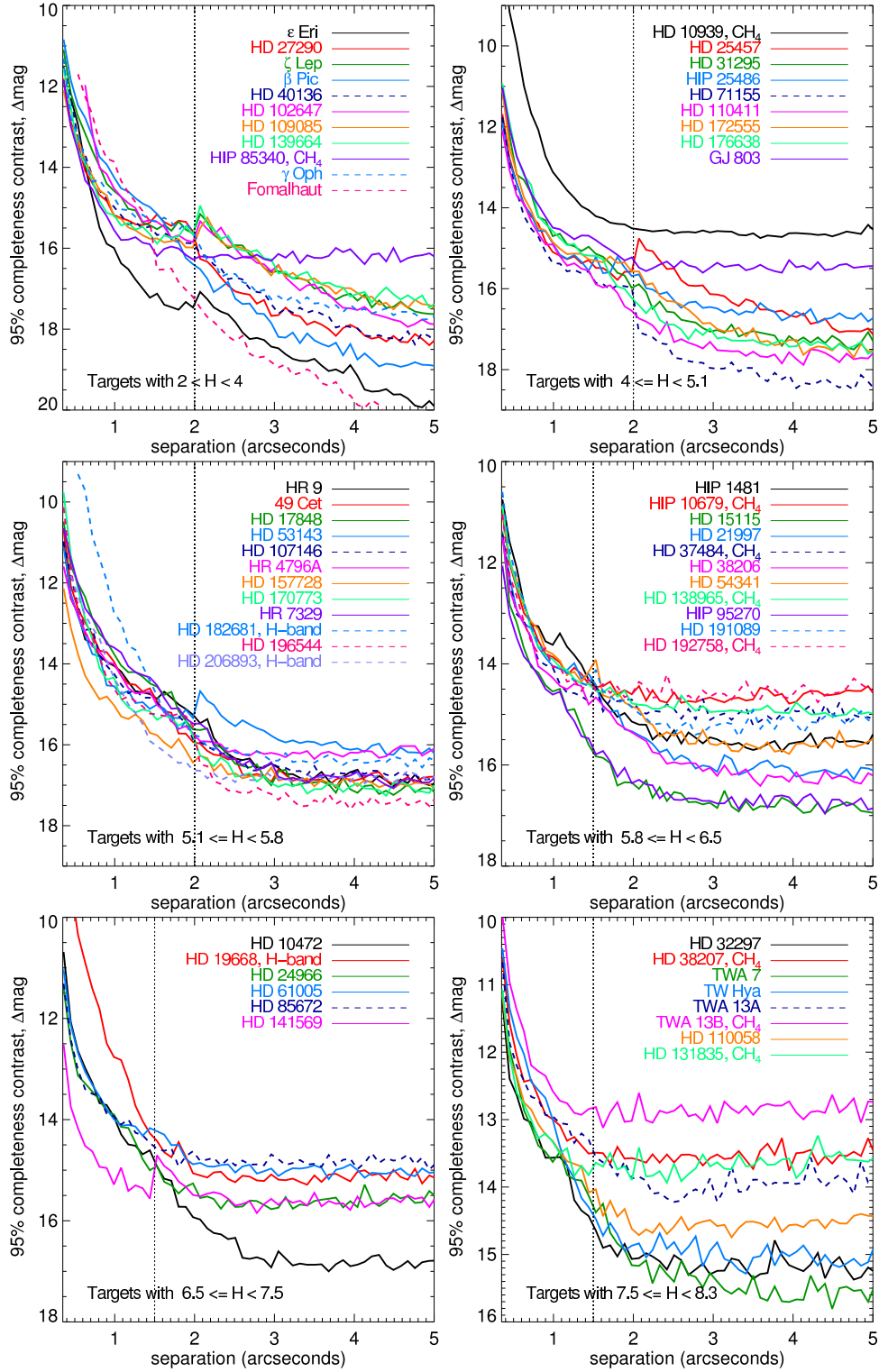


Fig. 2.— The contrast curves for all Campaign debris disk targets, categorized by H -band magnitude of the primary. For separations less than $\sim 1.5''$, the CH_4 filter contrasts are usually better. For larger separations, the H -band contrasts are better. In the figure above, beyond the dotted-line we show the H -band contrasts. When only one filter is available, the star’s name in the legend is tagged with the filter name.

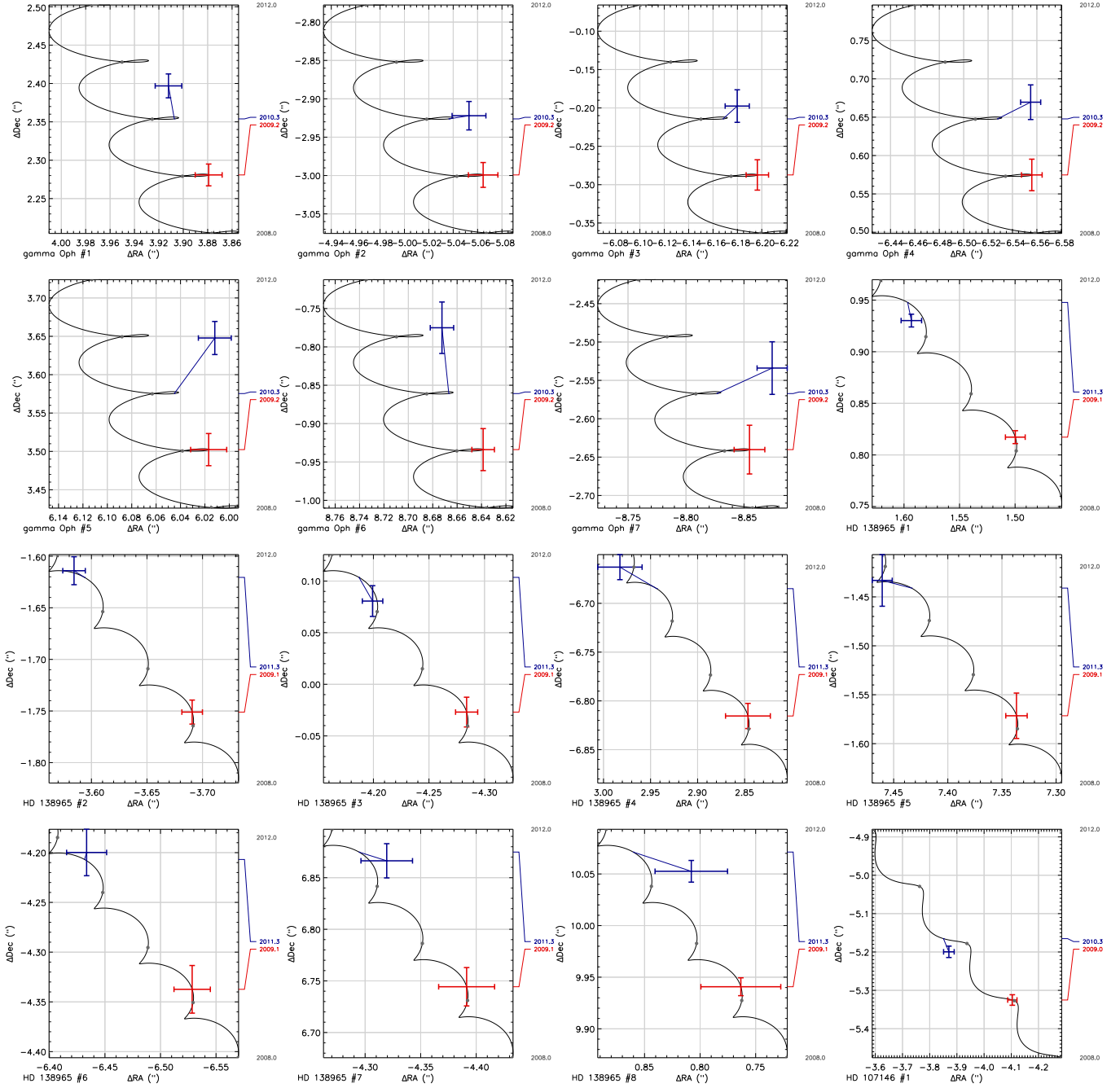


Fig. 3.— The change in RA and DEC of candidate companions around our target stars compared with the expected change for a background object, given the parallax and proper motion of the primary star. The error bars represent the uncertainty in our astrometry.

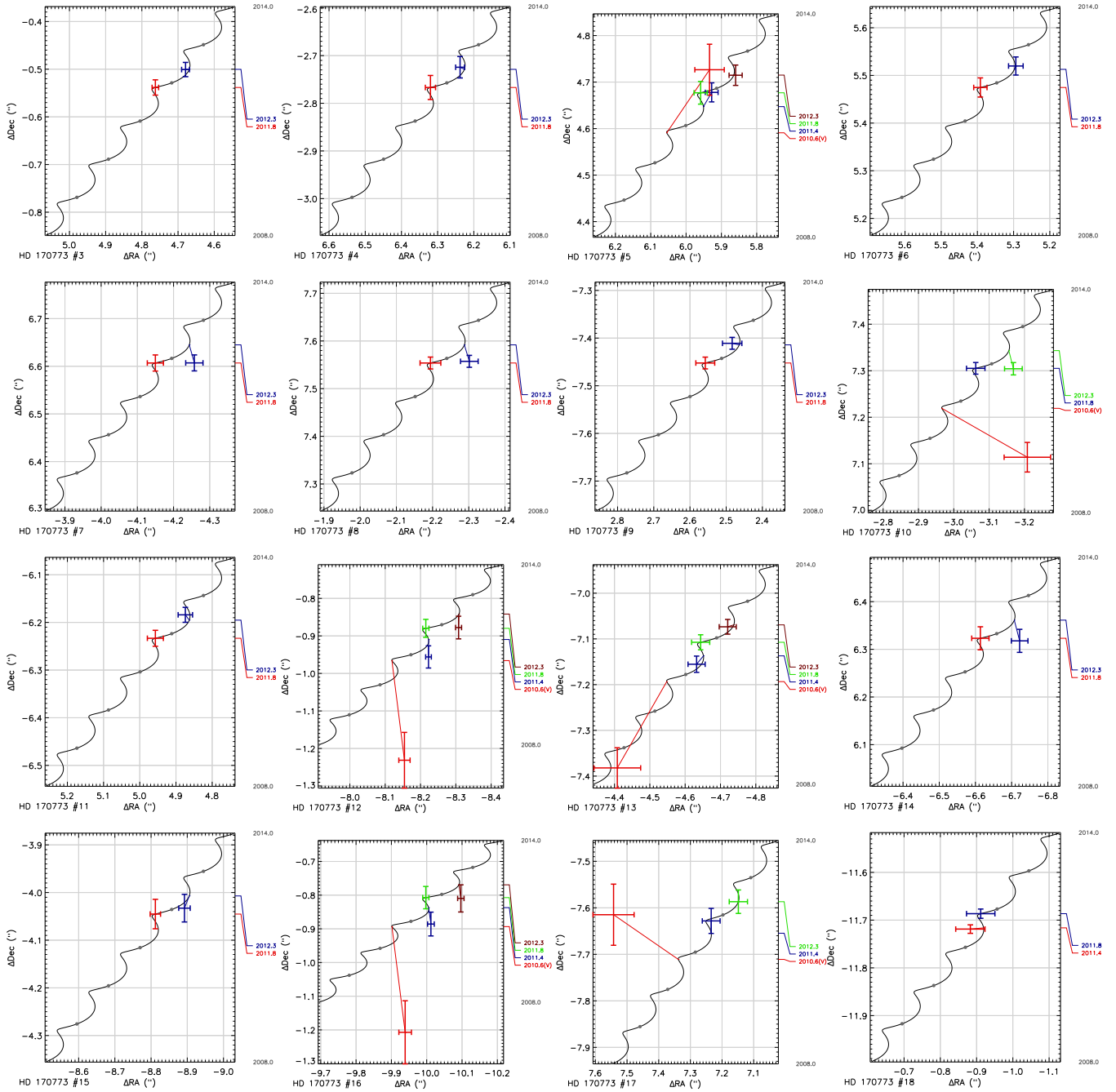


Fig. 4.— Same as Figure 3.

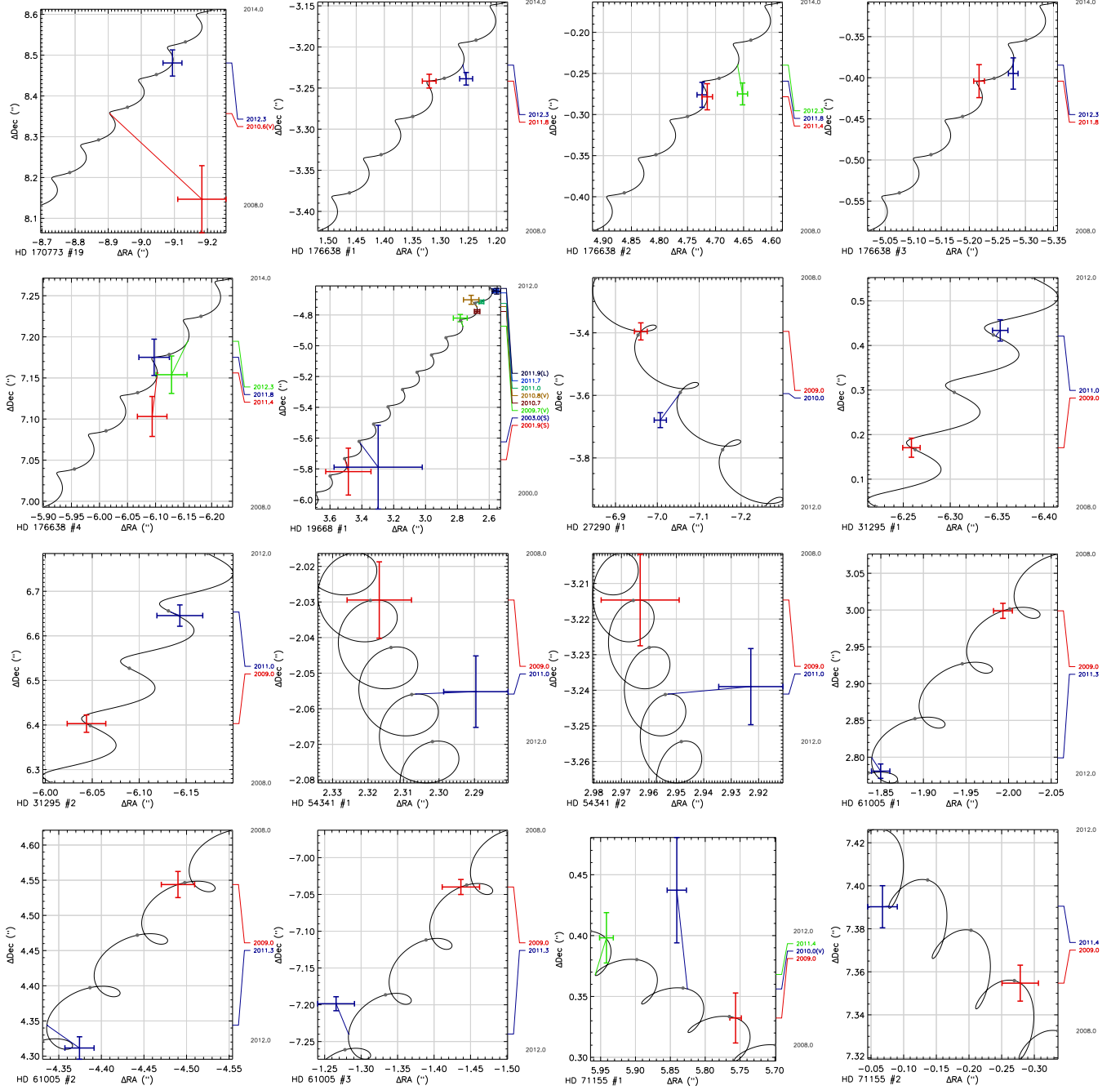


Fig. 5.— Same as Figure 3.

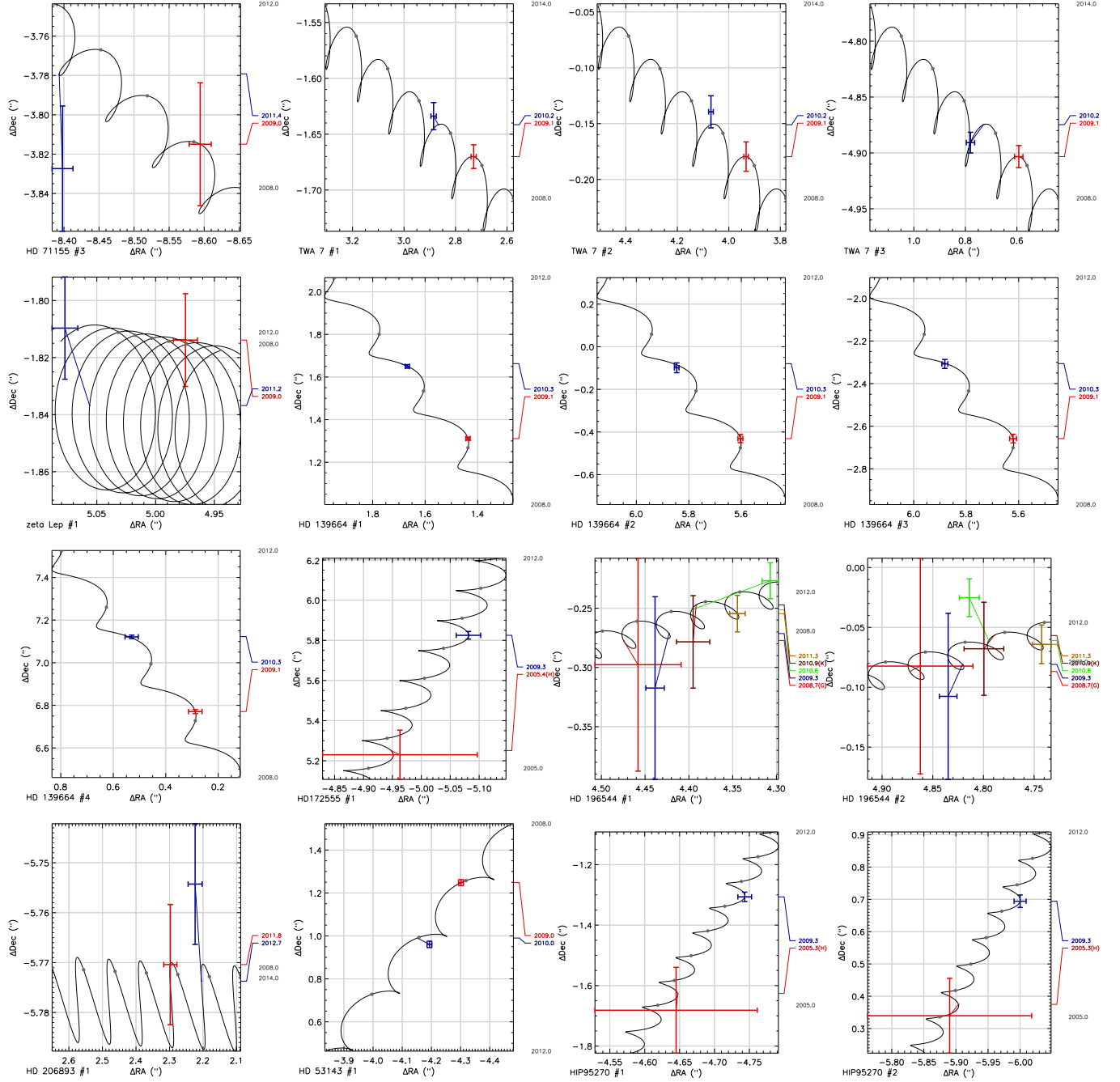


Fig. 6.— Same as Figure 3.

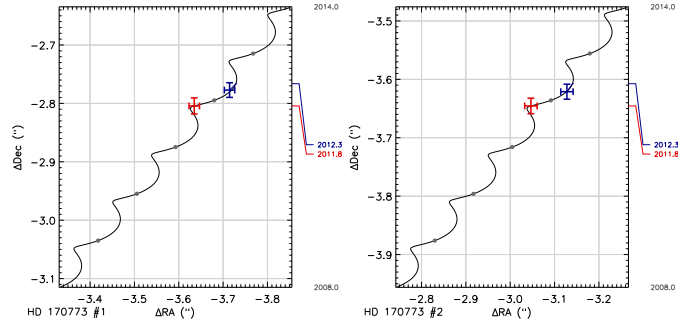


Fig. 7.— Same as Figure 3.

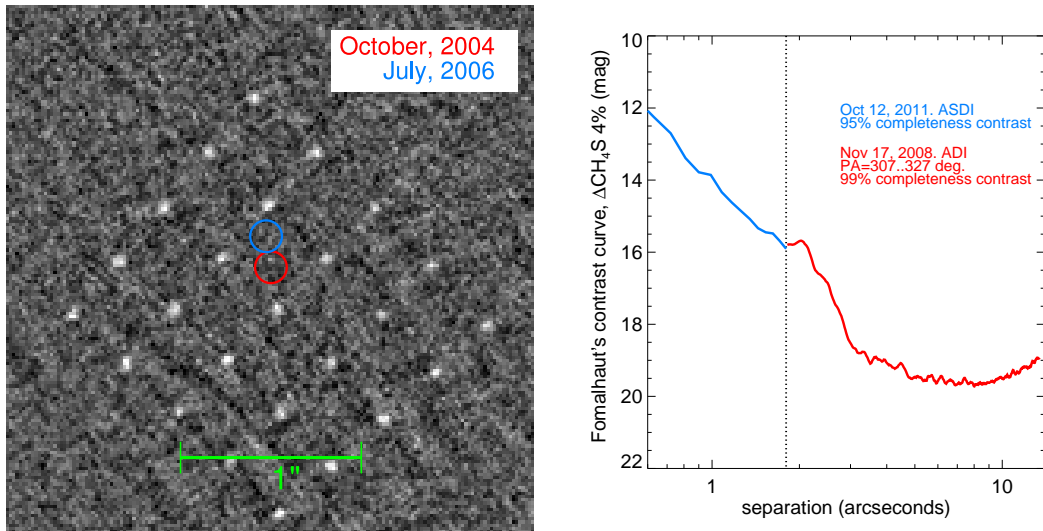


Fig. 8.— Left: CH_4S 4% NICI reduced image of Fomalhaut obtained on UT 2008 November 17, showing the locations of Fomalhaut b detections from Kalas et al. (2008). Also shown are simulated planets at the detection limit of the image at 20.2 mag. Right: Contrast curves from the data sets obtained UT 2011, October 12 and UT 2008, November 17, joined at a separation of 1.8". The 2008 contrast curve has been adjusted for anisoplanatism.

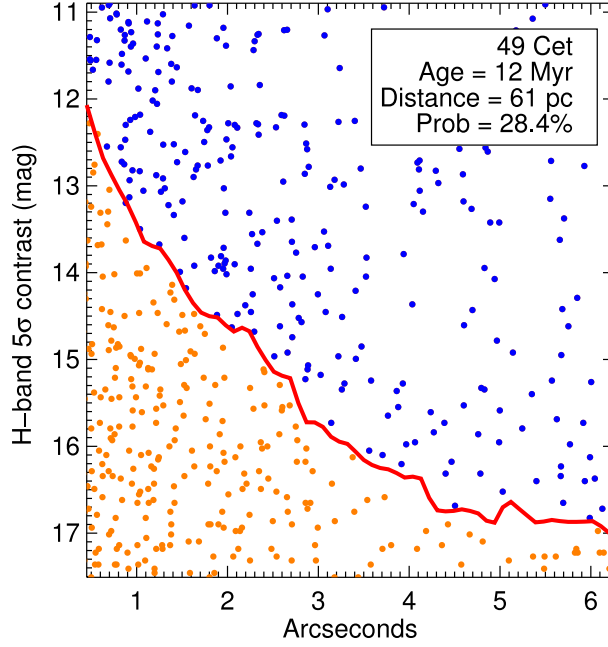


Fig. 9.— Simulated planets around 49 Cet. The red line is the 95% completeness contrast we achieved for 49 Cet. The blue dots represent planets which would have been detected by the Campaign observations, if they existed. The orange dots represent planets which would not be detected. The probability of detecting a planet, assuming that exactly one planet exists around 49 Cet is 28.4%. These are the f_j values we use in our Bayesian computations. The mass and SMA power-law indices, α and β , were set to -1.1 and -0.6 , respectively for the planet population model used in this particular simulation.

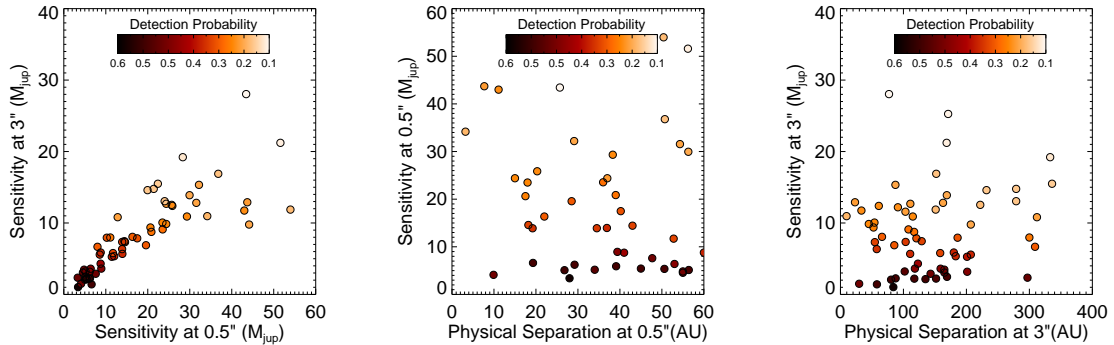


Fig. 10.— Comparison of the mass sensitivities reached at $0.5''$ and $3''$ and the detection probabilities, f_j .

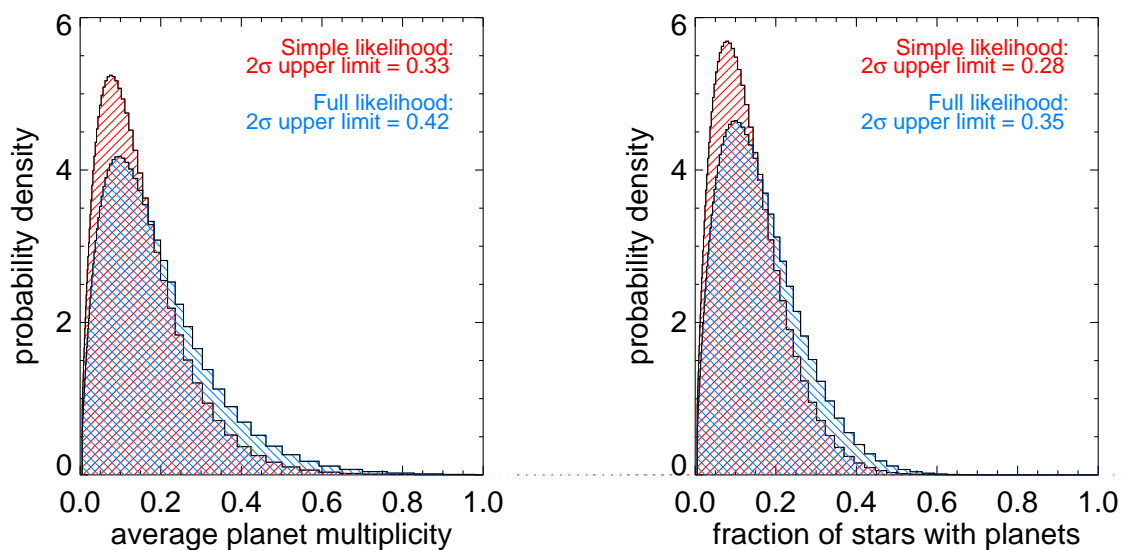


Fig. 11.— Left: The probability distribution for the average number of planets in systems with detected debris disks, F , when $\alpha = -1.31$ and $\beta = -0.61$ are set from Cumming et al. (2008). The distribution shown in red results from the simple likelihood where only the average number of planets detected is considered. The distribution in blue results from the full likelihood where the number of detections around a star is also considered. Right: The probability distribution for the fraction of stars with planets, F_{sp} .

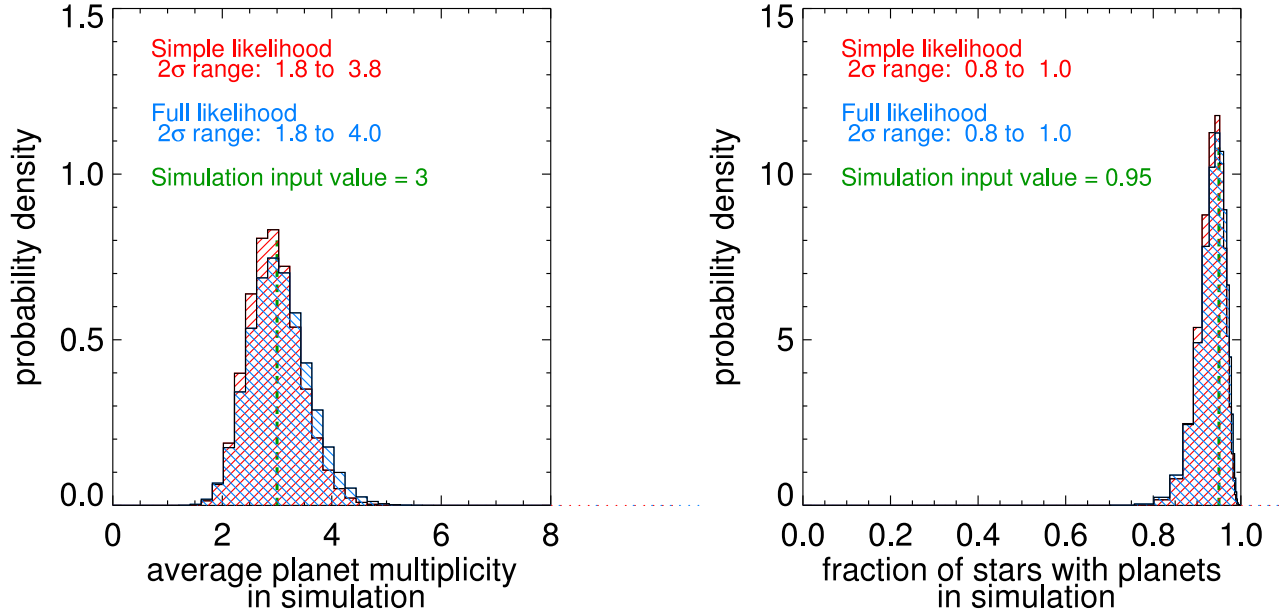


Fig. 12.— Probability distributions for the planet population from a simulation where the average planet multiplicity was 3, when $\alpha = -1.31$ and $\beta = -0.61$ are set from Cumming et al. (2008). Left: The probability distribution obtained for the average number of planets (F) in the simulated population. The distribution shown in red results from the simple likelihood, while the distribution in blue results from the full likelihood. Right: The probability distribution for the fraction of stars with planets (F_{sp}) in the simulated population. For $F = 3$, F_{sp} should be 0.95. The consistency our results with the input simulated population demonstrates the robustness of our Bayesian method.

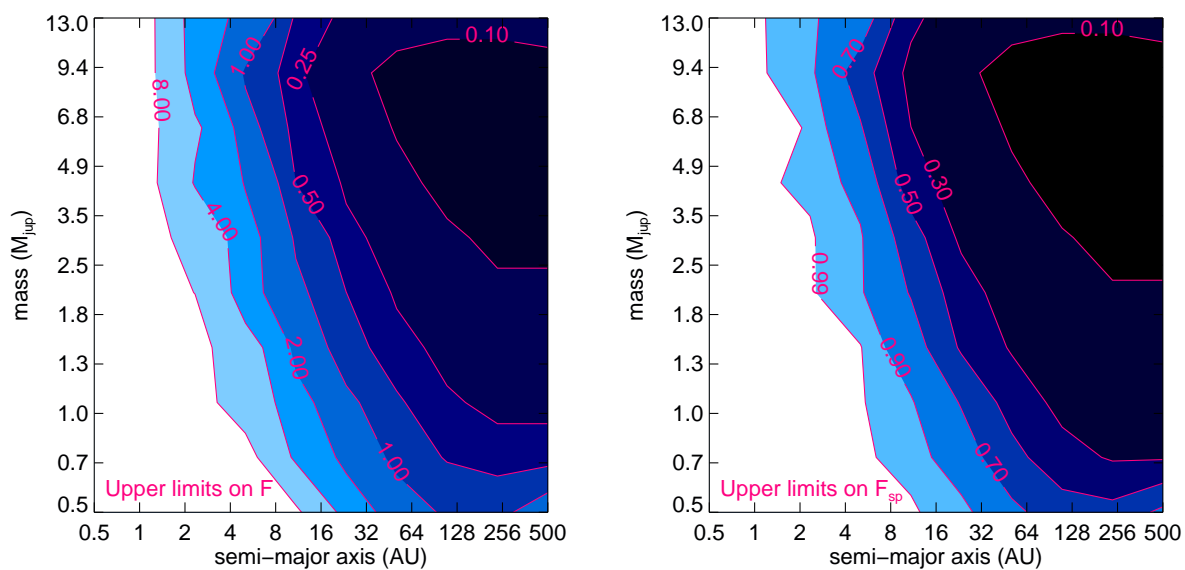


Fig. 13.— Left: The 2σ upper limits on the average number of planets in systems with detected debris disks, F , as a function of planet mass and orbital semi-major axis. Right: The 2σ upper limits on the fraction of stars with planets, F_{sp} , which is only valid for very small F or when stars are only allowed to have either one or zero planets. Again, the upper limits are given as a function of planet mass and SMA.

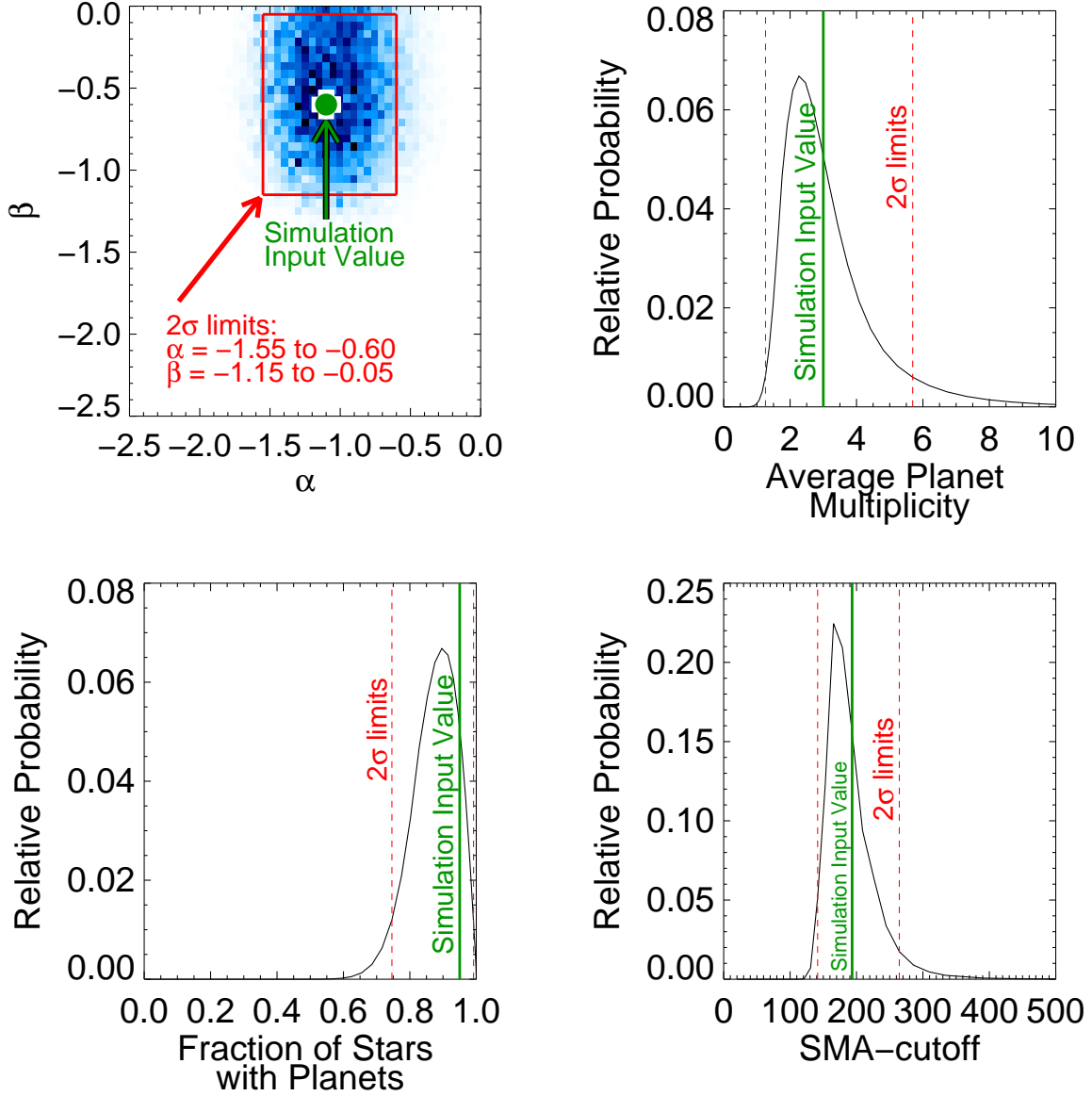


Fig. 14.— Constraints from a simulated survey where the input planet population has $\alpha = -1.1$ and $\beta = -0.6$, an average planet multiplicity of 3.0 and SMA cutoff of 193 AU. Darker regions indicate higher probability. Both astrometry and photometry of the model and simulated data are compared. Figures from left to right: the probability distributions for (1) the planet mass and SMA power-law indices, α and β (joint distribution), (2) the average planet multiplicity, (3) the fraction of stars with planets, and (4) the SMA cutoff beyond which no planets are allowed. The 2σ constraints from the Bayesian analysis are indicated by the red lines. The consistency of our results with the input simulated population demonstrates the robustness of our Bayesian method.

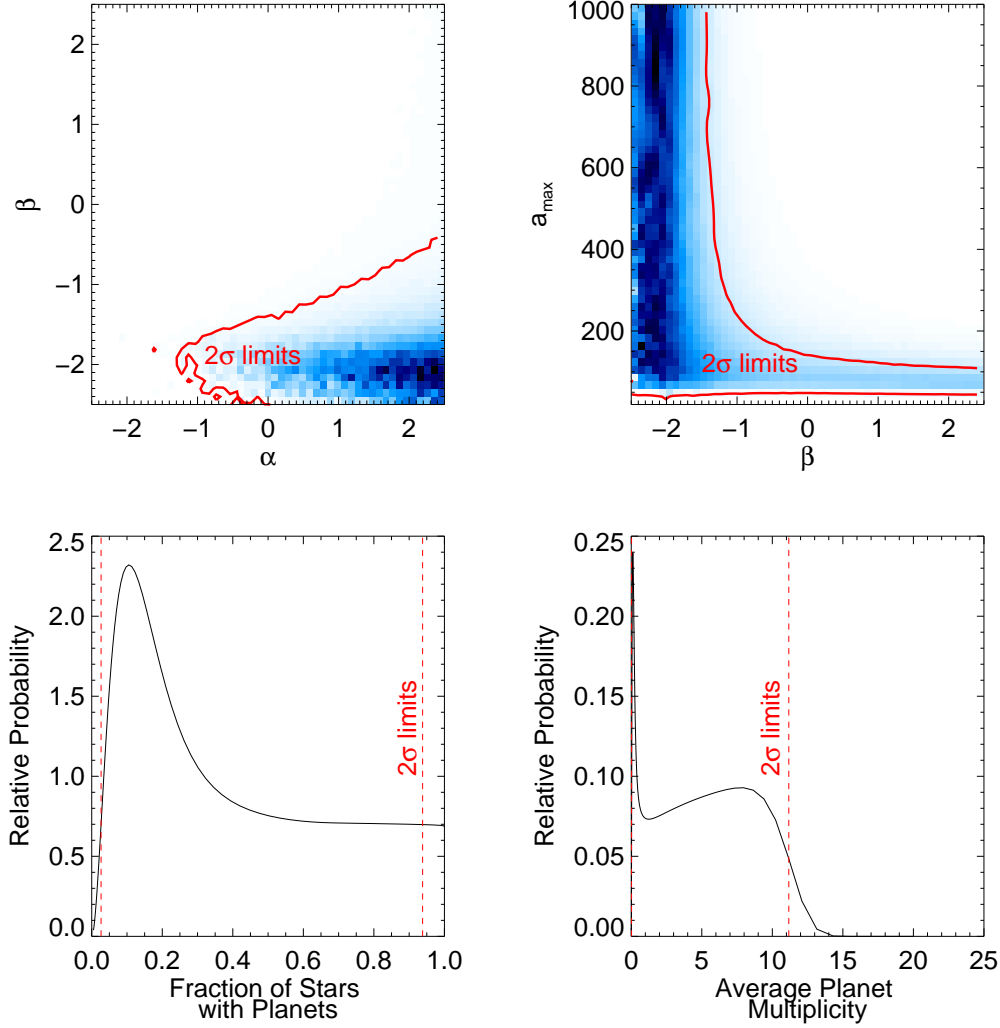


Fig. 15.— Constraints from the NICI debris disk survey combined with the Vigan et al. 2012 debris disk survey. Darker regions indicate higher probability. We include the planets β Pic b and HR 8799 bcd in this analysis. Figures from left to right: the probability distributions for (1) the planet mass and SMA power-law indices, α and β (joint distribution), (2) SMA power-law and SMA cutoff (joint distribution), (3) the fraction of stars with planets, and (4) the average multiplicity. The 2σ constraints from the Bayesian analysis are indicated by the red lines. Where the constrained space is degenerate in two parameters, as in the top two panels, we quote the constraints as follows. From the point $\beta = -0.8$ and $\alpha = 1.7$ on the 2σ rejection line, we can state that either $\beta < -0.8$ or $\alpha > 1.7$ (rising). With similar logic, we can state that either $\beta < -0.8$ or $a_{max} < 200$ AU.

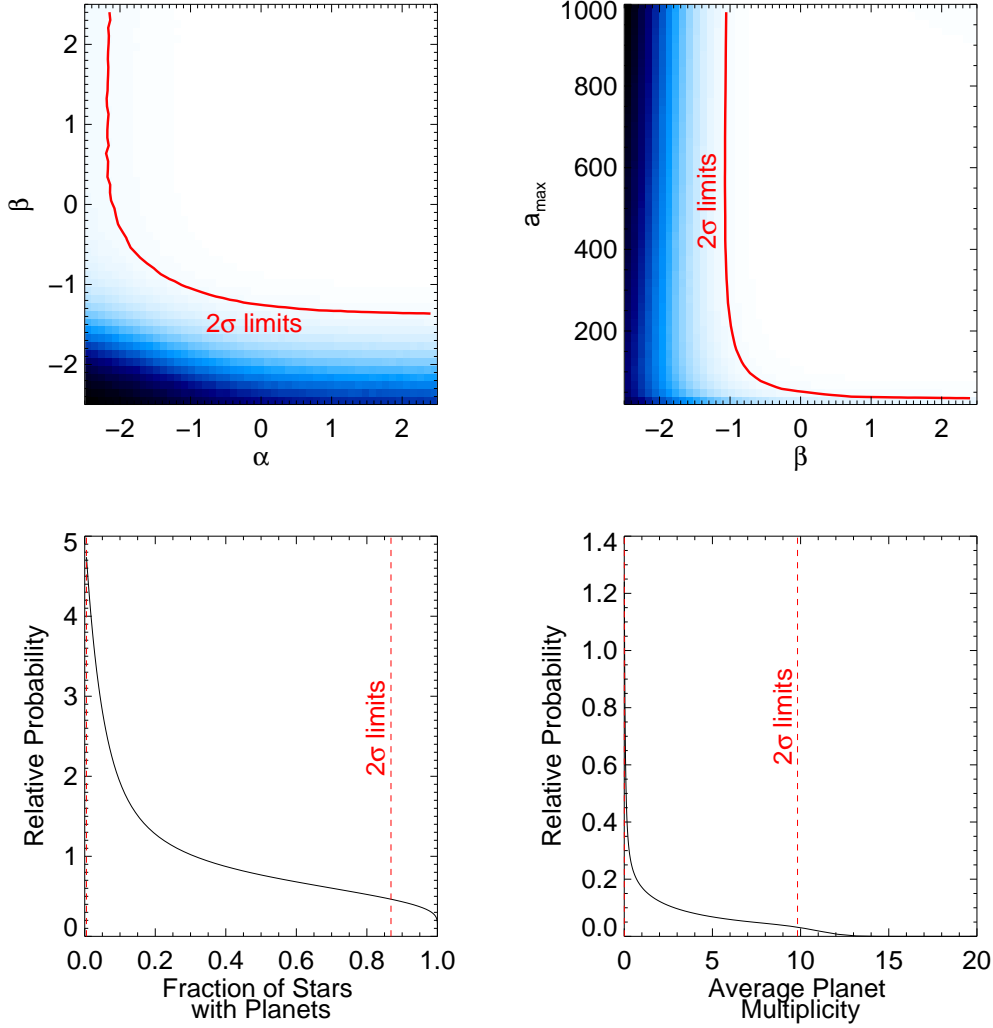


Fig. 16.— Constraints from the NICI debris disk survey combined with the Vigan et al. 2012 debris disk survey. Darker regions indicate higher probability. Here, we ignore β Pic b and the HR 8799 bcd planets. Figures from left to right: the probability distributions for (1) the planet mass and SMA power-law indices, α and β (joint distribution), (2) SMA power-law and SMA cutoff (joint distribution), (3) the fraction of stars with planets, and (4) the average multiplicity. The 2σ constraints from the Bayesian analysis are indicated by the red lines. Where the constrained space is degenerate in two parameters, as in the top two panels, we quote the constraints as follows. From the point $\beta = -0.8$ and $\alpha = -1.5$ on the 2σ rejection line, we can state that either $\beta < -0.8$ or $\alpha < -1.5$. With similar logic, we can state that either $\beta < -0.8$ or $a_{max} < 125$ AU.

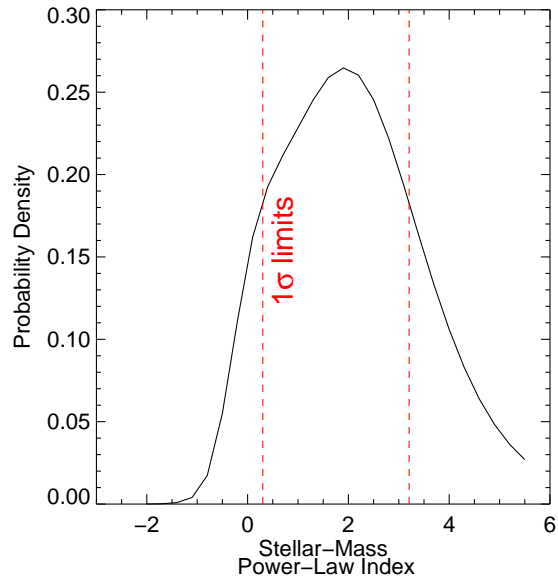


Fig. 17.— Constraints on the spectral-type power-law index from the augmented NICI debris disk survey, which includes β Pictoris b and the HR 8799 planets from the Vigan et al. (2012) survey. The 1σ limits on the index are $[0.3, 3.2]$. Thus an A5V star is predicted to have 1.2 to 9.2 times more planets than a G2V star.